Dalton Transactions

ROYAL SOCIETY OF CHEMISTRY

PAPER

View Article Online
View Journal

Cite this: DOI: 10.1039/d6dt00242k

Interactions of IOX1, a histone demethylase inhibitor, with essential metal ions, albumin, and its clay-based nanoformulation

Hilda Kovács, [a] Orsolya Dömötör, [a] Anett Giricz,[a] Nóra Igaz, [b] Krisztina Szőke,[b] Csenge Bocz,[b] Mónika Kiricsi, [b] Adél Szerlauth, [c] Réka Ormos,[c] István Szilágyi [c] and Éva A. Enyedy *[a]

Herein, the chemical properties of 5-carboxy-8-hydroxyquinoline (IOX1), a histone lysine demethylase KDM4 inhibitor, were comprehensively characterized in aqueous solution, including its complex formation equilibria with essential metal ions such as Fe(II), Fe(III), and Cu(II). IOX1 shows the following metal ion preference at pH 7.4: Fe(II) < Fe(III) < Cu(II). Compared to 2-oxoglutarate, the natural substrate of KDM4, IOX1 exhibits a higher affinity for both iron ions. The Rh(III)(η^5-C_5Me_5) (RhCp*) complex of IOX1 was synthesized and characterized by UV-visible, NMR, and mass spectrometry techniques, showing high stability in aqueous solution without the dissociation of IOX1 over a wide pH range and strong interaction with human serum albumin. To access the potential benefits of nanocapsulation, IOX1-loaded anionic clay (LDH) nanoparticles (LDH/IOX1) were successfully synthesized. The anticancer properties of IOX1, its RhCp* complex, and LDH/IOX1 were evaluated in human cancer cell lines. The RhCp* complex exhibited a greater antiproliferative activity toward Colo205 cells than IOX1 alone, and all tested compounds significantly decreased the mitochondrial membrane potential. The LDH/IOX1 system also showed pronounced cytotoxicity on A549 cells, accompanied by strong mitochondrial impairment, indicating the potential of nanocapsulation of small-molecule enzyme inhibitors in cancer therapy.

Received 30th January 2026,
Accepted 1st April 2026

DOI: 10.1039/d6dt00242k

rsc.li/dalton

Introduction

Chemotherapy remains one of the most common treatment strategies for various types of cancer, despite its well-known side effects. Among small-molecule anticancer compounds, several act as metalloenzyme inhibitors that disrupt enzymatic functions, often by coordinating to the metal ion at the active site. Although carbonic anhydrase (CA)[1] and matrix metalloproteinase (MMP) inhibitors[2] are structurally and mechanistically distinct, they share a common feature: the ability to inhibit enzymes that play crucial roles in cancer progression. Consequently, targeting metalloenzymes with selective inhibitors offers a promising approach in the development of novel anticancer therapies. Overexpression of histone lysine demethylase (KDM) enzymes is a common feature in various types of cancer, as these enzymes play an important role in regulating gene transcription and DNA repair.[3] KDM enzymes are classified into two major groups based on their catalytic mechanisms: one comprises flavin adenine dinucleotide (FAD)-dependent amine oxidases, while the other includes JmjC-domain-containing demethylases (JmjC-KDMs), such as the KDM2–KDM8 families, which are 2-oxoglutarate (2-OG, Fig. 1) and Fe(II)-dependent dioxygenases.[4]

Compounds containing the 8-hydroxyquinoline (HQ) scaffold have a wide variety of biological activities, including antibacterial,[5] antiviral, and anticancer properties.[6–8] For

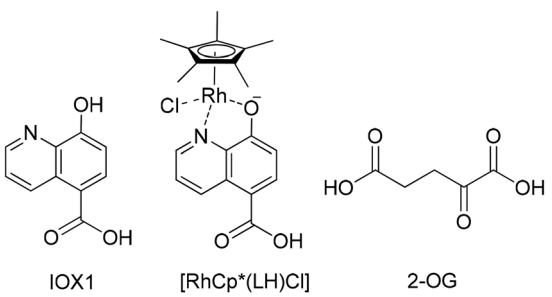

Fig. 1 Chemical structure of the studied molecules: IOX1 (in its neutral form, H_2L), RhCp* complex of IOX1 ([RhCp*(LH)Cl]), and 2-OG.

[a]*Department of Molecular and Analytical Chemistry, University of Szeged, Dóm tér 7-8., H-6720 Szeged, Hungary. E-mail: enyedy@chem.u-szeged.hu*
[b]*Department of Biochemistry and Molecular Biology, University of Szeged, Közép fasor 52, H-6726 Szeged, Hungary*
[c]*MTA-SZTE "Momentum" Biocolloids Research Group, Department of Physical Chemistry and Materials Science, University of Szeged, Rerrich Béla tér 1, H-6720 Szeged, Hungary*

example, 5-nitro-8-hydroxyquinoline is an approved drug for urinary tract infections, while 5-chloro-7-iodo-8-hydroxyquinoline is an FDA-approved antifungal agent.[9] One of the most notable HQ-based compounds is the tris-(8-quinolinolato) gallium(III) complex, also known as KP46. It is an orally administered anticancer drug in clinical trial phase I/II and has shown signs of effectiveness in treating advanced or recurrent solid tumors, including those affecting the breast, non-small cell lung, and prostate cancer.[10,11] The potential of other non-essential metal complexes of HQs as anticancer compounds has also been investigated, including those of Pt(II)[12] and Pd (II),[13] among others. Organometallic complexes of HQs, such as half-sandwich Rh(III)(η^5-C_5Me_5) (RhCp*) complexes, are also widely investigated for their potential in cancer therapy.[14–17] The pharmacokinetic properties of HQ ligands can be efficiently improved through complex formation, as the resulting water-soluble half-sandwich complexes are capable of binding to human serum proteins *via* coordination bonds.[14,15,18] Due to the strong metal-chelating ability of HQ derivatives *via* (N, O^-) donor atoms, several studies reported a relationship between their biological activity and metal-binding properties.[19–21] A series of HQ derived Mannich bases exhibited increased anticancer activity against multidrug-resistant cell lines, and it has been suggested that their mechanism of action is related to their complexation with essential metal ions, such as copper or iron, within the intracellular environment.[8,19,22]

Among the KDM4 inhibitors, some 8-hydroxyquinoline-based compounds can also be found. Most small-molecule inhibitors act by chelating the catalytic Fe(II) in the active site of the enzyme, thereby blocking the binding of the co-substrate molecule 2-OG, and ultimately suppressing KDM4 activity.[3] In our previous work, the HQ-based KDM4 inhibitor *N*-(3-(dimethylamino)propyl)-4-(8-hydroxyquinolin-6-yl)benzamide (ML324) was studied, which contains a positively charged side chain at position six. ML324 was found to have a higher affinity for Fe(III) over Fe(II); however, it is also capable of forming stable Fe(II) complexes at physiological pH 7.4.[23] 5-Carboxy-8-hydroxyquinoline (IOX1, Fig. 1) is a wide-spectrum 2-OG-dependent enzyme inhibitor. It inhibits the demethylation of histone lysine residues by chelating the Fe(II) in the enzyme's active site and competing with 2-OG.[24] IOX1 suppressed colorectal cancer tumorigenesis through inhibition of KDM3.[25] *In vivo* experiments have found that IOX1 inhibits the growth of colorectal tumors in mice, and it is even more effective when used in combination with the monoclonal antibody drug bevacizumab.[26] Although the mechanism of action of IOX1 involves the coordination to the Fe(II) center, no detailed information on its iron-binding ability is available in the literature. An evaluation of the direct interaction between this enzyme inhibitor and Fe(II) can therefore contribute to a better understanding of the inhibition mechanism.

IOX1, due to the negatively charged carboxylate group, can be a substrate of human serum albumin (HSA). HSA is the most abundant plasma protein in human blood and serves as a carrier for numerous drugs; binding to this transport protein has a strong impact on the pharmacokinetic behavior.[27,28] Drugs bound to macromolecules, including HSA, and other nanosized particles can accumulate in tumor tissue due to the enhanced permeability and retention (EPR) effect.[29] Layered double hydroxides (LDHs), also known as anionic clays, are biocompatible nanomaterials that have gained considerable attention as drug delivery systems. Several drugs can be loaded into LDHs, which increases their therapeutic effect for the treatment of various diseases, including cancer.[30,31]

In this study, we have characterized the behavior of IOX1 in aqueous solution, including its proton dissociation processes, lipophilicity, complex formation equilibria with Fe(II) and other essential metal ions, such as Fe(III) and Cu(II), as well as the redox properties of iron and copper complexes. For comparison, we studied the interaction of 2-OG with Fe(II) and Fe (III), as 2-OG serves as the natural substrate of the KDM4 enzyme. Since the formation of metal complexes with bioactive compounds can lead to altered mechanisms of action and improved pharmacokinetic properties, such as enhanced protein-binding affinity, we synthesized and characterized the Rh(III)(η^5-C_5Me_5) (RhCp*) complex of IOX1 (Fig. 1). This strategy has already been successfully applied in our previous works.[14,32] The interaction of IOX1 and its RhCp* complex with HSA was also studied. Moreover, the nanoformulation potential of IOX1 using LDH nanoparticles was explored. The cytotoxic and antiproliferative activity of IOX1, its RhCp* complex, and the LDH-loaded IOX1 formulation was evaluated in A549 and Colo205 human cancer cells. In addition, their potential synergistic effects with metal chelators, namely 3-hydroxy-1,2-dimethylpyridin-4(1*H*)-one (deferiprone, an iron chelator) and ammonium tetrathiomolybdate (TTM, a copper chelator), were also investigated.

Results and discussion

Solution chemical properties of IOX1

As the physico-chemical properties of a compound are known to influence its pharmacokinetics, it is important to investigate its lipophilicity and protonation state at physiological pH. The completely protonated form (LH_3^+) of IOX1 contains three dissociable protons: the quinolinium nitrogen (N_qH^+), the carboxyl group (COOH), and the hydroxyl group (OH). This compound has a relatively good intrinsic solubility in water (S_0 = 1.2 mM);[33] however, its copper and iron complexes are less soluble. Therefore, pH-potentiometry could not be used to study the deprotonation and complexation process in pure aqueous solution, as this method requires even higher concentrations. Therefore, pH-potentiometric titrations of IOX1 were carried out in a 30% (v/v) DMSO/H_2O solvent mixture, whereas UV-visible (UV-vis) spectrophotometric titrations could be performed in aqueous solution. The first two deprotonation processes could not be clearly resolved in the UV-vis spectra recorded (Fig. 2a), therefore, ^{1}H NMR titration was also carried out in a 10% (v/v) D_2O/H_2O mixture in the pH range 2.0–11.6 (Fig. S1a). The three pK_a values determined by the different

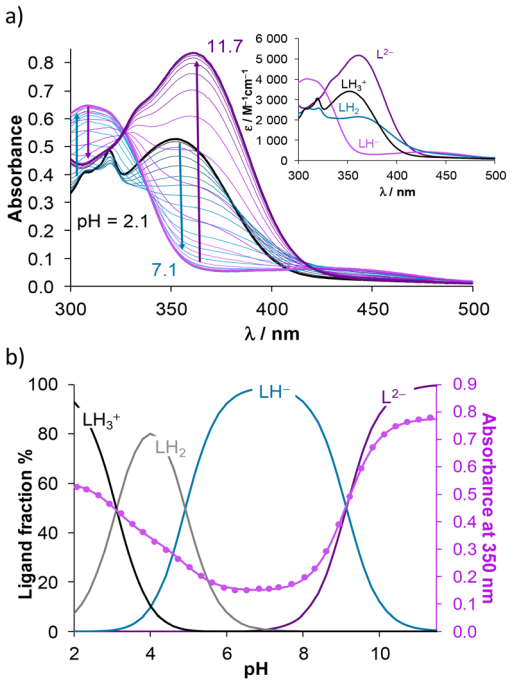

Fig. 2 (a) UV-vis absorption spectra recorded for IOX1 in the pH range 2.1–11.7, and the inserted figure shows the individual molar absorbance spectra of the ligand species in the different protonation states. (b) Concentration distribution curves calculated with the pK_a values obtained by UV-vis titrations, and absorbance changes at 350 nm (●) at various pH values with the fitted curve (solid line). {c_{IOX1} = 161 μM; ℓ = 1 cm; I = 0.1 M (KCl); T = 25.0 °C}.

methods are shown in Table 1. Due to the chromophore scaffold, deprotonation processes are accompanied by significant spectral changes, especially in the case of the deprotonation step $LH^- \rightarrow L^{2-}$, resulting in the development of a strong absorption band ($\lambda_{max} \sim 362$ nm) that is typical for the dissociation of the OH group.[18] Thus, we suggest that pK_3 cleary belongs to this moiety. ^{1}H NMR spectroscopy serves as a valuable method to identify the deprotonation processes. The results revealed that the C7H proton, located near the OH group, is fairly sensitive to deprotonation, as are the C6H and C2H protons situated close to the COOH and quinolinium nitrogen atoms, respectively. The first two deprotonation processes overlap and cannot be assigned unambiguously to individual moieties. Therefore, pK_1 and pK_2 are considered as macroscopic constants. However, based on our findings and comparison with the pK_a values of related ligands (such as 4-hydroxybenzoic acid, benzoic acid, phenol, HQ),[18,34] the quinolinium nitrogen is the most acidic site, and deprotonation starts there, followed by the COOH group. The pK_a values of both the quinolinium nitrogen and the hydroxyl group are lower than those of HQ (N_qH^+: 4.78, OH: 9.74 (ref. 18)) due to the electron withdrawing effects of the COOH (affecting N_qH^+) and COO^- (affecting mostly OH) substituents.

The COOH group exerts strong –I and –M effect, decreasing the basicity of the quinolinium nitrogen, whereas the COO^- group, with its much weaker –I and resonance donating (+M) character, has a more moderate influence on the acidity of the hydroxyl group, consequently the decrease is greater for the pK_a of N_qH^+ than for the phenolic OH. Concentration distribution curves were calculated using the three pK_a values determined (Fig. 2b), showing the predominance of the LH^- species at pH 7.4. It should be noted that the determined pK_a values of IOX1 in 30% (v/v) DMSO/H_2O solvent mixture and in water are slightly different. According to the Born electrostatic solvent model,[35] the pK_a of cationic acids decreases, whereas that of neutral acids increases in the presence of DMSO compared to water, due to isoelectronic and charge neutralizing protonation processes. In our case, the pK_a value associated with the neutral hydroxyl group (pK_3) indeed increases in the less polar solvent; however, the pK_a of the COOH group (~pK_2) remained almost unchanged, and that of the quinolinum nitrogen (~pK_1) was unexpectedly increased in the presence of DMSO. It seems that the electron-withdrawing COOH group already reduced the basicity of the quinolinium nitrogen to such an extent that further solvent-induced stabilization effects became negligible, in addition to the partial overlap of the proton dissociation equilibria in the acidic pH range.

Lipophilicity of IOX1 was also characterized; distribution coefficients (log D) were determined by n-octanol/water partitioning at two different pH values, and $\log D_{2.0} = +0.1 \pm 0.1$ and $\log D_{7.4} = -1.3 \pm 0.1$ were obtained at pH 2.0 and 7.4, respectively. The pronounced hydrophilicity at pH 7.4 is due to the predominating negatively charged LH^- species. The reference compound HQ has a more lipophilic character at pH 7.4 ($\log D_{7.4} = +1.81$ (ref. 18)), since it is present in its neutral form at this pH.

The inhibitory activity of IOX1 arises from its competition with 2-OG at the enzyme active site,[24] the natural substrate of the KDM4 enzyme, and the solution chemical properties of the 2-OG were also investigated for comparison. To characterize the deprotonation processes of 2-OG (which possesses two dissociable protons in its fully protonated form, Fig. 1), pH-potentiometric and UV-vis spectrophotometric titrations were performed. Using the first method, we determined the pK_a value for the second deprotonation process as 4.62 ± 0.05. However, this technique did not provide reliable information for the first process, since it occurs in the strongly acidic pH range (pK_a < 2), where the glass electrode's acid-error limits accurate measurement. The obtained pK_a value for the second deprotonation process is in a good agreement with the litera-

Table 1 pK_a values of IOX1 determined by pH-potentiometric titration in 30% (v/v) DMSO/H_2O and UV-vis spectrophotometric titrations in water. {T = 25.0 °C}

	pH-Potentiometry	UV-vis	^{1}H NMR
Solvent	30% (v/v) DMSO/H_2O	H_2O	10% (v/v) D_2O/H_2O
Ionic strength	0.1 M KCl	0.1 M KCl	0.2 M KNO_3
pK_1	3.35 ± 0.06	3.12 ± 0.03	3.19 ± 0.03
pK_2	5.05 ± 0.04	4.92 ± 0.03	4.88 ± 0.03
pK_3	9.62 ± 0.03	9.14 ± 0.03	9.13 ± 0.03

ture data.[36] However, in our opinion, the value of the first pK_a cannot be determined by pH-potentiometric titration due to methodological limitations. In contrast, using UV-vis spectrophotometric method in the pH range 1.4–8.2 (Fig. S2), both pK_a values could be determined (Table S1). (Notably, in this case the pH is calculated at pH < 2 on the basis of the strong acid content of the samples.)

Complexation of IOX1 with essential metal ions

Since the inhibition mechanism of IOX1 is thought to be linked to the coordination to the active Fe(II) center of the enzyme KDM4, the complex formation equilibria of IOX1 with Fe(II) was investigated and supplemented with other essential metal ions such as Fe(III) and Cu(II). In order to study the complex formation of IOX1 with Fe(III) and Fe(II), UV-vis spectroscopic titrations were carried out at different metal-to-ligand ratios, and for Fe(II) a laboratory glove box was used to provide strictly anaerobic conditions. During the titrations of the ligand with Fe(III), the absorbance values tend to decrease at pH > 8, as the hydrolysis of Fe(III) suppresses the formation of IOX1 complexes. The spectra recorded at different pH values indicate that Fe(II) and Fe(III) can form mono-, bis- and tris-ligand complexes in solution under the conditions used (Fig. 3). The overall stability constants obtained from the experimental data are shown in Table 2. In the case of Fe(III), protonated mono- and bis-ligand complexes were also formed under acidic conditions, in which the protons were attributed to the non-coordinating COOH group. For all iron complexes, it has also been suggested that the ligand is coordinated through the (N,O$^-$) donor group, based on spectral changes similar to those observed in Fe(III) complexes of HQ (*e.g.* tris-complex: λ_{max} = 455 and 582 nm).[37,38] The concentration distribution curves (Fig. 3b and d) reveal that the tris-ligand complexes predominate at pH 7.4 for both iron ions.

Spectra were also recorded for the Cu(II)–IOX1 system in the pH range 1.9–11.6 (Fig. S3) at different metal-to-ligand ratios to determine the speciation model and formation constants

Table 2 Overall stability constants (log β) of IOX1 complexes formed with Cu(II), Fe(II) and Fe(III) determined by UV-vis spectrophotometric titrations along with pM values (−log[M], where [M] is the equilibrium concentration of unbound metal ion) computed at c_L = 10 μM and c_M = 1 μM at pH 7.4 and pM values for the HQ complexes for comparison[a] {*T* = 25.0 °C; *I* = 0.1 M (KCl)}

log β	Cu(II)[b]	Fe(II)	Fe(III)[b]
[M(LH)]	16.14 ± 0.06	—	16.30 ± 0.04
[ML]	13.90 ± 0.03	7.88 ± 0.02	—
$[M(LH)_2]$	—	—	31.98 ± 0.03
[M(LH)L]	28.43 ± 0.05	—	—
$[ML_2]$	24.05 ± 0.04	15.40 ± 0.02	23.92 ± 0.05
$[ML_3]$	—	21.56 ± 0.02	34.01 ± 0.06
pM/IOX1	16.4	7.9	9.3 (19.3)[c]
pM/ML324[d]	11.1	7.3	14.6 (24.6)[c]
pM/HQ[d]	15.1	—	10.3 (20.3)[c]
pM/HQS[d]	15.0	7.9	8.1 (18.1)[c]

[a] Charges of the complexes are omitted for clarity. L^{2-} is doubly negatively charged. [b] Data were evaluated at pH < 9. [c] pFe(III) = −log([Fe^{3+}] + $[Fe(OH)]^{2+}$ + $[Fe(OH)_2]^+$ + $[Fe(OH)_3]$ + $[Fe(OH)_4]^-$ + $[Fe_2(OH)_2]^{4+}$), the number in the brackets shows the pM value when pFe(III) = −log[Fe^{3+}] as traditionally calculated. [d] Overall stability constants for pM calculation were taken from ref. 23 and 37.

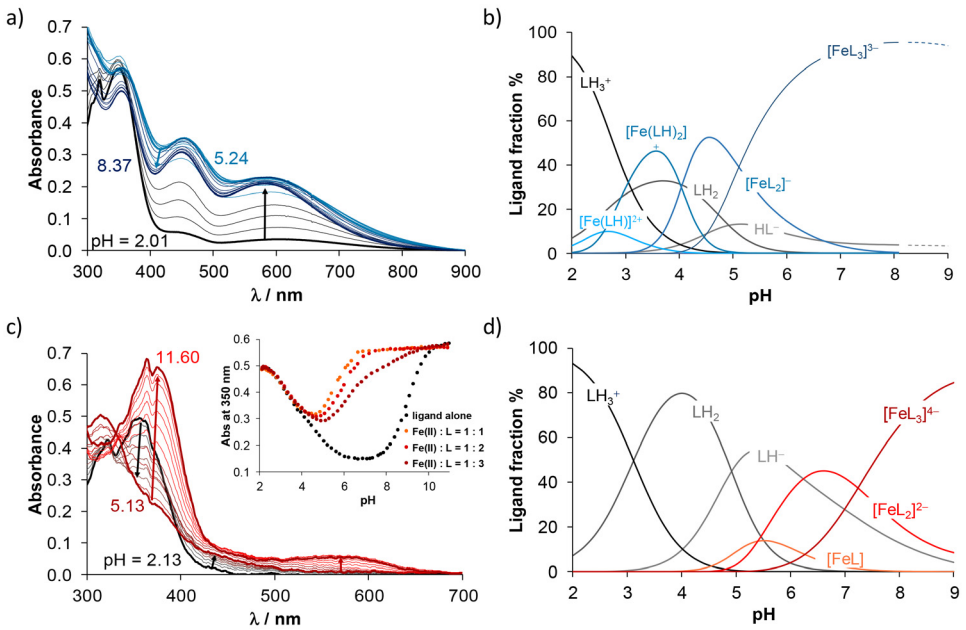

Fig. 3 UV-vis absorption spectra recorded for the (a) Fe(III)–IOX1 (1 : 3) system in the pH range 2.0–8.9 and for the (c) Fe(II)–IOX1 (1 : 3) system in the pH range 2.1–11.6, inserted figure shows the absorbance values measured at 350 nm at various metal-to-ligand ratios. Concentration distribution curve calculated for the same systems: (b) Fe(III)–IOX1 and (d) Fe(II)–IOX1. {(a): c_{IOX1} = 161 μM, $c_{Fe(III)}$ = 53 μM; (c): c_{IOX1} = 151 μM; $c_{Fe(II)}$ = 50 μM; ℓ = 1 cm; *I* = 0.1 M (KCl); *T* = 25.0 °C}.

(Table 2). As expected, mono- and bis-ligand complexes are formed with Cu(II), as with the reference compound HQ.[39] Due to the nature of the spectral changes, formation of mono-ligand complexes $[Cu(LH)]^+$ and $[CuL]$, in addition to bis-ligand species $[Cu(LH)L]^-$ and $[CuL_2]^{2-}$, were suggested. Based on the calculated concentration distribution curves (Fig. S3b), the bis-ligand $[CuL_2]^{2-}$ complex is the predominant species at pH 7.4.

Based on the overall stability constants of the complexes with the studied essential metal ions (Table 2), the highest values were found for Fe(III) and Cu(II). However, the metal ion preference of ligands cannot be evaluated solely by comparing the overall stability constants, as the metal ions form diverse types of complexes and exhibit varying affinities for hydroxide ions. Thus, pM values were calculated at pH 7.4 for appropriate comparison, and hydrolysis constants of the metal ions were also taken into consideration (Table 2). The higher pM value indicates a stronger preference of the ligand for metal ions; consequently, the metal ion affinity of IOX1 follows the order: Fe(II) < Fe(III) < Cu(II). A similar trend in metal ion preferences is observed for both HQ and 8-hydroxyquinoline-5-sulfonic acid (HQS).

Among the studied metal ions, IOX1 has the lowest affinity for binding Fe(II), however, it is still capable of forming complexes with Fe(II) at pH 7.4, which may be sufficient for effective enzyme inhibition. If we compare IOX1 to another 8-hydroxyquinoline derivative KDM4 inhibitor ML324, both compounds show a stronger preference toward Fe(III) than Fe (II).

Natural substrate of KDM4, 2-OG complexation with Fe(II) and Fe(III) were also studied, and the determined overall stability constants were collected in Table S1. In the case of Fe(II), pH-potentiometric titrations were performed, and data were evaluated at pH < 7 due to the hydrolysis of Fe(II).

No available data were found in the literature for the complex formation in the Fe(II)–2-OG system, the obtained data were compared to those of the Fe(II)–malonic acid system. Overall stability constants were determined in different medium (I = 1.0 M $NaClO_4$) for mono- and bis-ligand complexes of malonic acid ($\log\beta$[ML] = 2.17 and $\log\beta$[ML2] = 3.21),[40] revealing quite low stability. The stability constant for the $[Fe(II)LH]^+$ complex of 2-OG, in which the non-coordinating carboxyl group is still protonated, could be determined in our work only with high uncertainty. Based on this constant, the complex is present in the solution between pH 1.5 and 6, and its maximum fraction is 10% reached at pH *ca.* 3. Complex formation of 2-OG with Fe(III) was studied by UV-vis spectroscopic titrations. The obtained experimental data were evaluated at pH < 4, since at higher pH values a precipitate formed due to the strong hydrolysis of Fe(III), indicating low complex stability. The precipitate was filtered and subsequently dissolved in 0.2 M HCl. ^{1}H NMR spectrum recorded for the sample confirmed that the precipitate corresponded to Fe(III) hydroxido species (since no ligand was present in the solution). Based on the changes in the UV-vis spectra, formation of $[Fe(III)LH]^{2+}$, $[Fe(III)L]^+$, and $[Fe(III)L_2]^-$ species with 2-OG was observed, the constants could be determined only with high uncertainty due to their low fractions (Table S1). Fig. S4 shows the spectra of ligand (2-OG) and Fe(III) alone in addition to the Fe(III)–2-OG (1 : 3) system at pH 1.4. Their difference indicates complex formation only at very acidic pH and to a fairly low extent. pH-Potentiometric data reported on complex formation of 2-OG with Fe(III)[41] showed even lower constants compared to our data (Table S1). These findings clearly indicate the much lower stability of the iron complexes of 2-OG compared to those of IOX1.

Redox properties of iron and copper complexes were characterized by cyclic voltammetry. A 60% (v/v) *N*-dimethylformamide (DMF)/H_2O solvent mixture was used due to the low aqueous solubility of the formed complexes. Cyclic voltammograms of Fe(III)–IOX1 (1 : 3) system were recorded at different scan rates at pH 7.4 (Fig. 4a), which displayed reversible electrochemical processes. Fig. 4b shows the linear dependence of the current on the square root of the applied scan rates, suggesting a diffusion-controlled process in both oxidation states. UV-vis spectra were measured at various potential values for the same solutions (Fig. 4c), and this spectroelectrochemical measurement also confirmed the reversibility of the processes. While for the Cu(II)–IOX1 (1 : 2) system, irreversible electrochemical processes were observed. Electrochemical data collection is found in Table 3, revealing negative formal potential values for both iron and copper complexes. These lower potential values indicate that IOX1 prefers the higher oxidation state forms of the metal ions (Fe(III) and Cu(II)). For comparison, cyclic voltammetric measurements were also performed on the Fe(III)–2-OG (1 : 3) system in 60% (v/v) DMF/H_2O solvent mixture, and electrochemical data were collected in Table 3. The experiment was done at pH 3, since precipitation occurred as the pH value was increased. Anodic and cathodic peaks were also observed in the voltammograms, but the electrochemical process was not reversible (Fig. S5). The peak position in the fairly negative potential range indicates that 2-OG has a higher affinity for Fe(III) than Fe(II), similarly to IOX1. The 2-OG ligand's preference for Fe(III) is not surprising given that it features an (O,O) donor atom set.

Synthesis and solution speciation of the RhCp* complex of IOX1

The RhCp* complex of IOX1 was obtained by reacting IOX1 with the $[Rh(III)Cp^*(\mu\text{-}Cl)Cl]_2$ precursor under basic condition in a methanol/chloroform solvent mixture, resulting in the deprotonation of the phenolic OH group. After workup, the product was isolated as [RhCp*(LH)Cl] in a good yield. To characterize the isolated organometallic half-sandwich complex (Fig. 1), ^{1}H, ^{13}C NMR spectroscopic and HR-ESI-MS techniques were used (see Experimental section and Fig. S6–S8). The experimental data confirmed that the complex has the composition [RhCp*(LH)Cl].

Stability of the isolated complex [RhCp*(LH)Cl] was investigated in modified phosphate-buffered saline (PBS′) at pH = 7.4 for 48 h by UV-vis spectrophotometry. The RhCp* complex of IOX1 showed no significant spectral changes during the

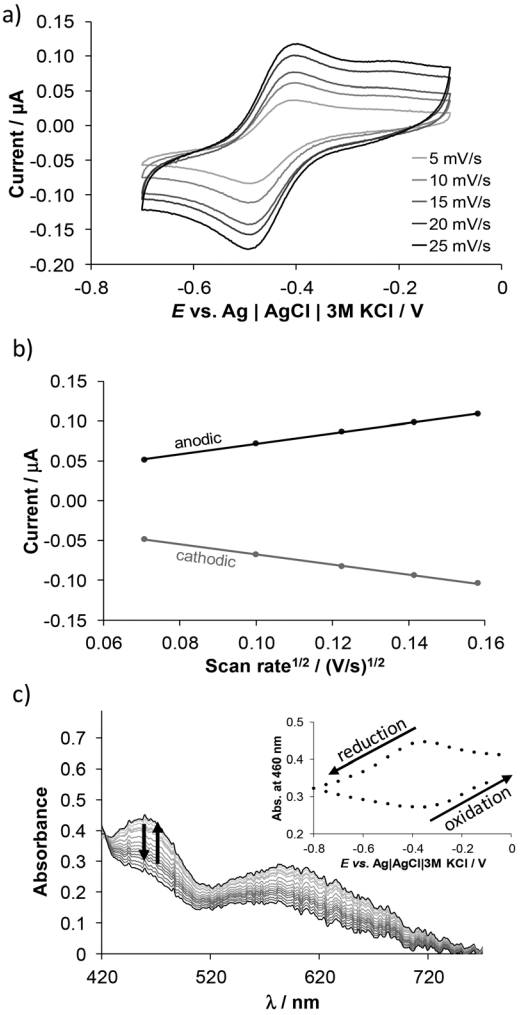

Fig. 4 (a) Cyclic voltammograms of the Fe(III)–IOX1 system at various scan rates (indicated in the figure). (b) Current is plotted against the square root of the applied scan rate for the same system. (c) For the same system UV–vis absorption spectra were recorded at different potential values by using the spectroelectrochemical cell kit at 10 mV s^{-1} scan rate. Inserted figure shows the absorbance values at 460 nm plotted against the potential. {c_{IOX1} = 1.5 mM; $c_{Fe(III)}$ = 0.5 mM; ℓ = 1.70 mm; pH = 7.4; 60% (v/v) DMF/H_2O; I = 0.1 M (KNO_3); T = 25.0 °C}.

Table 3 Electrochemical data collected for the iron–2-OG (1 : 3), iron–IOX1 (1 : 3) and copper–IOX1 (1 : 2) systems by the cyclic voltammetric measurements. {c_{ligand} = 1.5 mM; 60% (v/v) DMF/H_2O; scan rate: 10 mV s^{-1}; T = 25 °C; I = 0.1 M (KNO_3)}[a]

	2-OG[a]	IOX1[b]	
	Iron	Copper	Iron
E_c/V	−0.488	−0.486	−0.734
E_a/V	−0.378	−0.412	−0.595
ΔE/mV	110	73	139
$E_{1/2}$/mV	−402	−449	−665
$E_{1/2}$ *vs.* NHE/mV	−180	−227	−443
$\lvert i_a/i_c \rvert$	0.56	0.95	0.86

[a] Measured at pH = 3. [b] Measured at pH = 7.4.

studied period (Fig. S9a). Comparing the character of the spectra (λ_{max}, ε) to those of other related complexes,[14,18] IOX1 coordinates as a bidentate ligand *via* (N,O^-) donor set.

In order to better understand the solution phase behavior of the RhCp* complex of IOX1, equilibrium constants for the formation of the complex and for the deprotonation of the coordinated aqua ligand and the carboxyl group were determined. Moreover, the equilibrium constant for the possible chlorido/H_2O exchange process was also determined, using the same approach as in our previous works.[14,18] The complex formation was studied by mixing the $[RhCp^*(H_2O)_3]^{2+}$ cation with the IOX1 in a tandem cuvette in equimolar ratio at pH ~ 2 in the absence of chloride ions (0.01 M HNO_3). As expected, complexation was rapid at acidic pH also, with equilibrium reached in about 3 min (Fig. S9b), consistent with earlier reports on the fast formation of RhCp* complexes with 8-hydroxyquinolines.[14,15] Based on this finding, an aqueous solution of the complex was *in situ* prepared in further studies by mixing equimolar solutions of the RhCp* triaqua cation and IOX1 when chloride-free conditions were applied.

UV-vis titrations were performed for the $[RhCp^*(H_2O)_3]^{2+}$–IOX1 (1 : 1) system in the pH range of 2.3–11.3 also in the absence of chloride ions. It should be noted that the complex formation was quantitative at the initial pH. Two processes were observed based on the spectra as the pH values were increased (Fig. S10). The first belongs to the deprotonation of the carboxyl group of the coordinated ligand, and the second to the deprotonation of the coordinated water molecule. ^1H NMR spectroscopic titration was also carried out (Fig. 5), and we could observe the deprotonation step by monitoring the chemical shift of the protons located near the non-coordinating carboxyl group. Meanwhile, the chemical shift of the methyl groups of the Cp* ring is more sensitive to the deprotonation of the coordinated water molecule. The deprotonation of the carboxyl group of the complex occurs at a lower pH than in the case of the free ligand. The pK_a values determined by the different methods are given in Table 4. Based on these results, the complex is present in $[RhCp^*(L)(H_2O)]$ form (Fig. 5c) in aqueous solution at pH 7.4, at which the deprotonation of aqua co-ligand does not occur.

The fact that no dissociation of IOX1 ligand was observed from the complex at pH 2 indicates its high stability. A ligand replacement spectrophotometric study was performed to determine the conditional formation constant of the complex using 2,2′-bipyridine (bpy) as a competitor ligand (Fig. S11). The calculated conditional formation constant of RhCp*–IOX1 complex is $\log K'_{7.4} = 13.18 \pm 0.03$ at pH 7.4. Similar values were obtained for other RhCp*–8-hydroxyquinoline complexes, suggesting comparably high stability.[15,42]

At physiological pH (7.4), the predominant species of the complex is the $[RhCp^*(L)(H_2O)]$ form (in the absence of chloride ions). The aqua co-ligand can be exchanged in the presence of chloride ion, thus, the chloride ion affinity of the RhCp* complex of IOX1 was studied by UV-vis spectroscopy (Fig. S12). The calculated conditional exchange constants ($\log K'$ (H_2O/Cl^-)) are given in Table 4, and the data show that

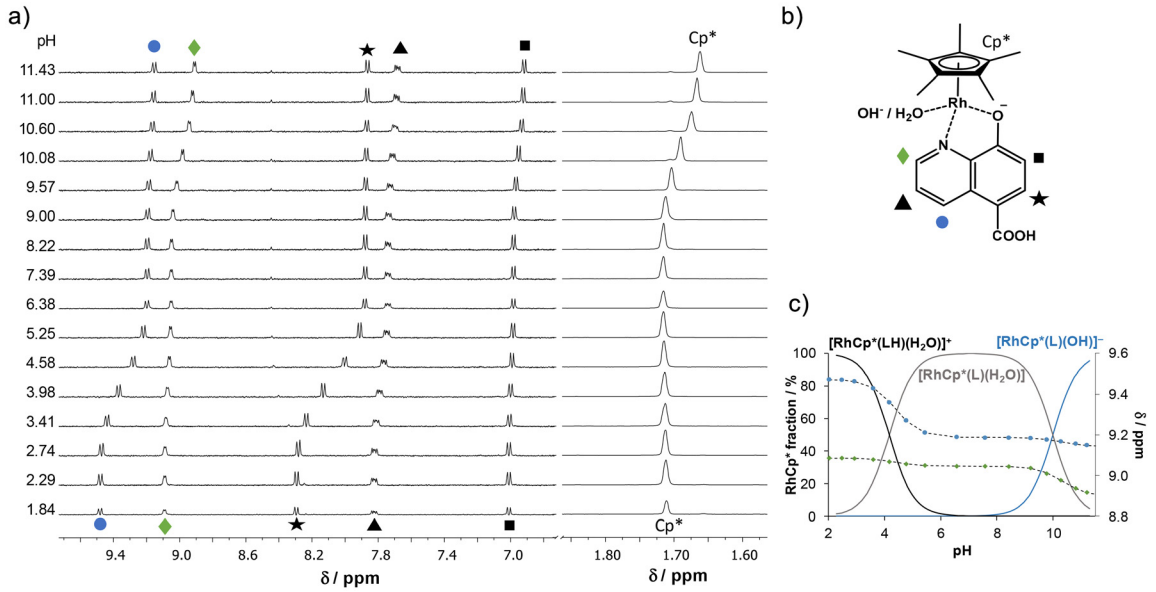

Fig. 5 (a) ^{1}H NMR spectra recorded for $[RhCp^*(H_2O)_3]^{2+}$–IOX1 (1 : 1) system in the pH range 1.8–11.4. (b) Chemical structure of the complex with the notation of the symbols of the protons. (c) Chemical shifts of two selected protons (●, ♦) at various pH values with the fitted curve (dashed lines). {$c_{RhCp^*} = c_{IOX1}$ = 500 μM; I = 0.2 M (KNO_3); 10% (v/v) D_2O/H_2O; T = 25.0 °C}.

Table 4 Collection of pK_a values of the *in situ* prepared RhCp* complex of IOX1 and its conditional H_2O/Cl^- exchange constant (log K' (H_2O/Cl^-)) determined at pH 7.4. {I = 0.20 M (KNO_3); T = 25.0 °C}

method	pK_a (COOH)	pK_a (H_2O)	log K' (H_2O/Cl^-)
UV-vis	4.15 ± 0.03	9.93 ± 0.03	1.48 ± 0.03
^{1}H NMR	4.17 ± 0.03	10.13 ± 0.03	—

the affinity for chloride ions is lower compared to that of similar HQ half-sandwich RhCp* complexes,[18] most likely due to the negatively charged carboxylate group in the coordinated ligand, similarly as it was also reported for 2-picolinate and 2,6-dipicolinate complexes.[43]

IOX1 and its RhCp* complex interaction with HSA

Human serum albumin can act as a carrier by reversibly binding the drug, which increases its biological half-life, since only the free fraction is susceptible to rapid metabolic processes and clearance. It is essential that the interaction with HSA is strong enough to prolong circulation, yet not so strong as to prevent the gradual release of the active compound.[28] Moreover, the HSA-bound drug may also accumulate in tumor tissues due to the enhanced permeability and retention effect. The albumin binding of IOX1 was investigated by a combination of spectroscopic (spectrofluorometry) and separation methods (ultrafiltration and equilibrium dialysis). Ultrafiltration conducted at 1 : 1 and 1 : 0.5 IOX1-to-HSA ratios shows considerable binding of IOX1 to the protein in Fig. 6a. Compared to related structures, quinoline-5-carboxylic acid (Q-COOH) and HQ bind with somewhat lower affinity to HSA,

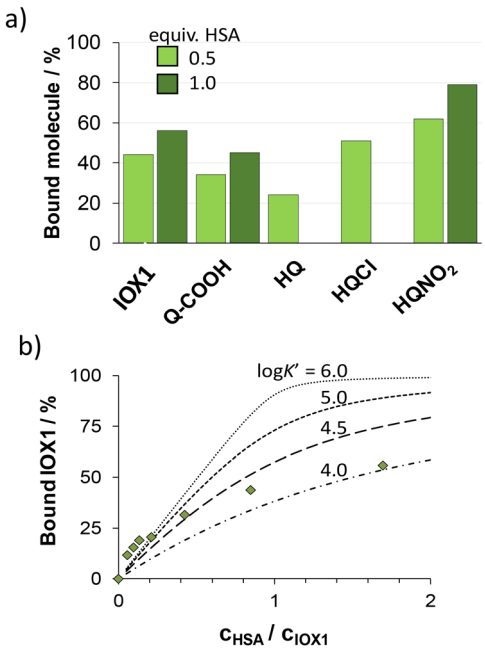

Fig. 6 (a) Bar chart of the bound compound fractions obtained in ultrafiltration – UV-vis studies in the indicated HSA–compound systems. HSA–HQCl and HSA–$HQNO_2$ systems were studied in ref. 43 (b) Bound IOX1 fractions in the HSA–IOX1 system determined by ultrafiltration (♦) and binding isotherms (black lines) calculated for one-site binding with the indicated binding strengths. {c_{comp} = 100 μM; pH = 7.4 (PBS′, 2 mM EDTA); T = 25 °C}.

showing the importance of both phenol and carboxylate functional groups in the binding interaction. HSA binding of IOX1 is weaker than that reported for 5-chloro-8-hydroxyquinoline

(HQCl) and 5-nitro-8-hydroxyquinoline ($HQNO_2$).[44] The binding isotherm in Fig. 6b comprises the data obtained at various HSA-to-IOX1 ratios in ultrafiltration experiments. At low HSA equivalents (0.06–0.13), bound IOX1 fractions exceed the maximum amount that can be bound by one binding site, also, the one-site binding models do not fit well to the experimental data, strongly suggesting the existence of at least two binding sites of IOX1 in HSA. The UV-vis spectrum of IOX1 was not sensitive to the HSA binding, therefore, spectrofluorometry was applied as next step.

Fluorescence quenching experiments exploit the sensitivity of Trp-214 located in site I (subdomain IIA) for binding events at or near this site of HSA. The intensive fluorescence of HSA (λ_{EM}(max) = 340 nm) was gradually quenched in Fig. 7 by the addition of IOX1. Concomitantly, a new emission band emerged at *ca.* 400 nm, which belongs to IOX1, and it is barely sensitive to the protein binding.

The quenching constant was calculated with HypSpec software[45] using the complete spectral range (300–500 nm), and a value of $\log K' = 4.9 \pm 0.1$ was determined. The interaction of IOX1 with fatty acid binding sites of HSA cannot be ruled out due to the presence of the carboxylate function. Trp-214 quenching experiments with fatty acid-free albumin provided the same quenching constant ($\log K' = 4.9 \pm 0.1$) as reported for the fatty acid-containing albumin, therefore, considerable interaction at these sites is not feasible.

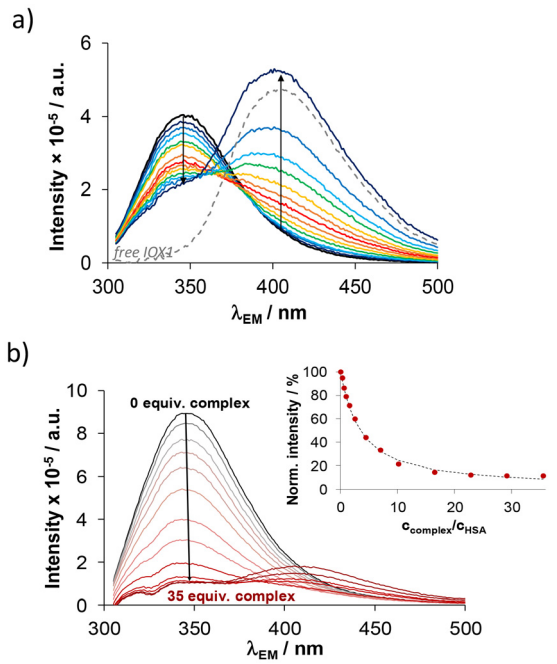

Fig. 7 Quenching of HSA fluorescence by (a) addition of IOX1 and emission spectrum of IOX1 alone (dashed spectrum, 60 μM); (b) addition of various amounts of the RhCp*–IOX1 complex. The inserted figure shows the quenching curve at 350 nm; the dashed line is the fitted titration curve. {c_{HSA} = 1 μM; (a): c_{IOX1} = 0–60 μM; (b): $c_{complex}$ = 0–35 μM; λ_{EX} = 295 nm; pH = 7.4 (PBS′, 2 mM EDTA); T = 25 °C}.

The site marker displacement experiments conducted with warfarin (WF, site I marker) and dansylglycine (DG, site II marker) indicated no considerable competition of IOX1 for these sites (Fig. S13). We further investigated the binding of IOX1 at the two hydrophobic pockets by the equilibrium dialysis method, applying on-line UV-vis detection in the acceptor phase.[32] The initial samples contained 100 μM HSA, 100 μM marker, and 200 μM IOX1. The respective HSA–compound binary systems and samples containing only IOX1, WF, or DG were prepared as well (Table S2). Recovery from the dialysis membrane was excellent for all compounds (≥96%). The time required to achieve equilibrium was *ca.* 6.5, 8.5, and 10 h for the HSA–IOX1, HSA–DG, and HSA–WF systems, respectively. Therefore, 10 h was applied for equilibration in the ternary systems. IOX1 has little effect on the HSA-bound fraction of WF and DG (see detailed data set in Table S2 and Fig. S14). In the case of WF, this insensitivity appears to be mutual, namely, the bound amount of IOX1 is barely affected by the presence of WF. The addition of DG increases the free amount of IOX1 from 30% to 39%; it must have an allosteric effect on the binding pocket of IOX1, since, as it was indicated above, IOX1 does not displace DG considerably (19% → 21%).

Considering the quenching constant as a binding constant, about 98% of IOX1 may be albumin-bound at physiological conditions (630 μM HSA, 1–100 μM IOX1). Overall, the albumin binding of IOX1 is significant, although the nature of the binding site(s) requires further investigation.

The interaction of the organometallic RhCp* complex of IOX1 with HSA was also investigated by UV-vis and spectrofluorometry methods. UV-vis spectra were followed in time for a sample with 1 : 0.5 complex-to-HSA, and spectral changes indicate an interaction between the complex and the protein (Fig. S15a). This type of half-sandwich can bind to HSA in a complex coordinated manner, presumably *via* the His imidazole nitrogen.[46,47] Therefore, 1-methylimidazole (MIM) was used as a binding model of HSA, as employed in our previous studies.[14,46,48] UV-vis spectra were recorded at 1 : 1 complex–MIM ratios, and similar spectral changes were observed as in the case of HSA (Fig. S16). This phenomenon suggests that the complex can form coordination bond(s) with albumin. The UV-vis spectra of the RhCp*–IOX1 complex in the presence of different equiv. MIM is shown in Fig. S16, based on the spectral changes, conditional constants ($\log K'$) were computed with MIM for the formation of mixed-ligand RhCp* complexes; namely, $\log K' = 5.2 \pm 0.1$. Spectrofluorometry was used to analyze the binding of the complex to albumin quantitatively. The Trp-214 quenching experiment was performed using a method similar to that used for IOX1, representative spectra shown in Fig. 7b. The quenching constant was $\log K' = 5.5 \pm 0.1$, this indicates that the RhCp* complex has a higher affinity for albumin than the IOX1 ligand alone.

Characterization of IOX1-loaded LDH nanoparticles

LDHs are a class of biocompatible nanomaterials that have received a great deal of attention as a potential carrier for drug delivery. LDHs can act as a drug reservoir, slowly releasing the

loaded compound in response to pH changes or physiological stimuli, improving its bioavailability. Therefore, we attempted to synthesize and characterize IOX1-loaded LDH nanoparticles. Given that the anionic (LH^-) form of IOX1 predominates at pH 7.4, based on its pK_a values, its intercalation into the LDH was expected.

The synthesis of IOX1-loaded LDH nanoparticles (LDH/IOX1) is detailed in the Experimental section. The crystal structure of LDH and LDH/IOX1 particles was investigated using X-ray diffraction (XRD) measurements (Fig. 8a). The diffractograms showed similar results to previous data with LDH nanoparticles, *i.e.*, the reflections confirmed the formation of a highly crystalline and phase-pure LDH-like structure.[49] The reflections were assigned to (003), (006), (009), (015), (018), (110), and (113) Miller indices. No shift in the (003) position occurred, indicating that IOX1 molecules did not intercalate between the layers. Besides, the half-width of the (003) reflection widened for the LDH/IOX1 composite.

As a consequence, the primer crystallite size decreased significantly after the addition of IOX1 to the synthesis mixture (Table S3). This observation, together with the change in peak intensity above 40°, indicates that IOX1 adsorption notably affected the lateral growth of the LDH crystallites.

The results of dynamic light scattering (DLS) and electrophoretic light scattering (ELS) measurements (Fig. 8b and Table S4) revealed that the hydrodynamic radius of LDH/IOX1 is larger by about 20 nm compared to bare LDH, while the zeta potential was slightly lower for the former particles. Such trends in size and charge imply that traces of particle aggregates might be present in the LDH/IOX1 sample, since the zeta potential is lower and thus, repulsion by the electrostatic double layers is weaker between the surfaces, leading to mild aggregation and a higher average hydrodynamic radius for the LDH/IOX1 sample.[50–52] The limited number of particle aggregates is also indicated by the small polydispersity indices, which were similar for both LDH and LDH/IOX1, referring to a relatively narrow particle size distribution.[53]

TEM images confirmed the typical hexagonal shape of the LDH[54] and LDH/IOX1 particles (Fig. S17). No significant change in morphology occurred after immobilization of the IOX1 molecules on the LDH surface, although the average size of the particles was increased from 41.7 ± 14.4 nm for LDH to 70.9 ± 26.8 nm for the LDH/IOX1 systems. These results were in good agreement with the hydrodynamic radius values determined by DLS studies.

UV-vis measurements were performed to characterize the structural features of LDH and LDH/IOX1 particles (Fig. S18). LDH showed no significant absorption band in the 200–800 nm range. In contrast, the IOX1 molecule exhibits three intense peaks (λ_1 = 230 nm, λ_2 = 313 nm, λ_3 = 445 nm). The absorption bands associated with IOX1 are clearly shifted ($\Delta\lambda_1$ = 28 nm, $\Delta\lambda_2$ = 50 nm, $\Delta\lambda_3$ = 21 nm) in the LDH/IOX1 composite, indicating the surface adsorption of the molecule.[55]

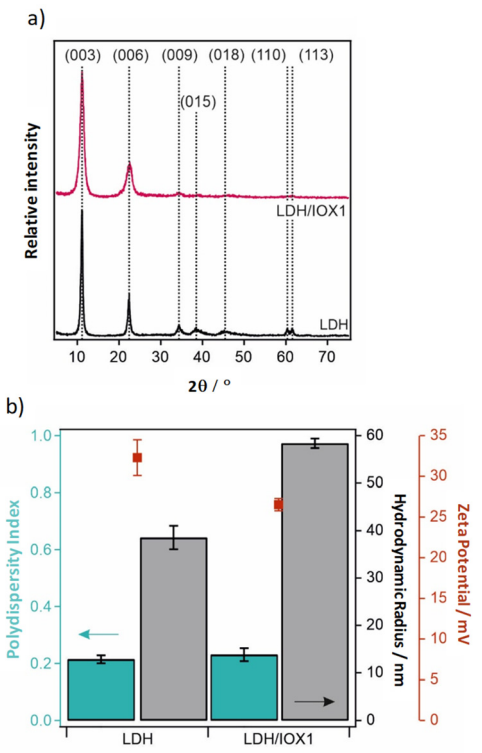

Fig. 8 (a) X-ray diffractogram and (b) hydrodynamic radius, polydispersity index, and zeta potential data of LDH and LDH/IOX1 particles.

Cytotoxic and antiproliferative effects of compounds on tumor cells

IOX1 was reported to inhibit KDM4A and other human 2-OG oxygenases with *in vitro* IC_{50} values in the micromolar range,[33,56] however, it exhibited only moderate-to-weak cytotoxic activity in HCT116 (colon cancer), MCF-7 (breast cancer), and A549 (lung cancer) cell lines.[56]

To detect the viability of A549 cells upon IOX1, [RhCp*(LH)Cl], LDH, or LDH/IOX1 treatments, 3-(4,5-dimethylthiazol-2-yl)-2,5-diphenyl tetrazolium bromide (MTT) assays were performed to monitor the impact of complex formation and nanoformulation with LDH on the cytotoxic activity of IOX1 using a shorter incubation period (24 h) (Fig. S19). At higher applied concentrations, all the tested compounds decreased the viability of A549 cells compared to the control samples. Notably, Feng *et al.* reported higher cytotoxicity for IOX1 on A549 cells (IC_{50} = 48.2 μM) compared to our results, however, they tested the cytotoxicity under other conditions (48 h incubation time and 4 × 10^3 cells per well *vs.* our case: 24 h incubation time and 10^4 cells per well).[33] According to the IC_{50} values (Table 5), the complexation with RhCp* increased the IC_{50} value of IOX1, while the loading into LDH decreased it.

As LDH treatment alone had also an impact on cell viability, the increased cytotoxicity of the LDH-loaded IOX1 can be attributed, at least in part, to the carrier itself. The cytotoxic effect of the compounds was also verified on A549 cells by the detection of cellular lactate dehydrogenase release, which is a sign of necrotic effects induced by the treatments. The IOX1

Table 5 IC_{50} values of the compounds were determined on A549 (24 h incubation time) and Colo205 (72 h incubation time) cells

	IC_{50} values/μM	
	A549	Colo205
IOX1	306.9 ± 1.08	45.56 ± 1.17
[RhCp*(LH)Cl]	389.9 ± 1.06	15.13 ± 1.52
LDH[a]	175.6 ± 1.09	—
LDH/IOX1[b]	217.9 ± 1.05	—
TTM	>400	—
Deferiprone	389.8 ± 1.05	—

[a] Here the IC_{50} value of LDH reflects only the cell response to the LDH dose corresponding to the 175.6 μM IOX1-equivalent loading, and should be interpreted as an indicator of carrier-associated effects rather than its intrinsic cytotoxicity. [b] The IC_{50} value is expressed with respect to the IOX1 concentration.

and [RhCp*(LH)Cl] did not affect the cell membrane integrity, similar lactate dehydrogenase activities were measured outside the cells, as in the case of the untreated control samples. Nevertheless, significant extracellular lactate dehydrogenase activity was obtained when the cancer cells were treated with either LDH/IOX1 or LDH (Fig. S20). These results suggest that IOX1 and [RhCp*(LH)Cl] are not or just slightly cytotoxic to A549 cells; however, LDH alone and LDH/IOX1 both induce a significant reduction in cell viability, which is the result, at least in part, of cell necrosis. MTT-based assays measure the viability of cells by determining their metabolic activity, with a significant contribution of mitochondrial enzyme activities requiring intact mitochondria.

Therefore, our next aim was to investigate the possible mitochondria-damaging effect of the compounds using 5,5′,6,6′-tetrachloro-1,1′,3,3′-tetraethyl-benzimidazolylcarbocyanine iodide (JC-1) staining. JC-1 is a membrane-permeable dye that selectively accumulates in mitochondria. When the mitochondrial membrane potential is maintained, JC-1 emits red fluorescence, but when the membrane potential is low, there is a shift in emission color from red to green. Upon the treatments of the A549 cells, all the tested compounds significantly decreased the mitochondrial membrane potential compared to the untreated samples. The lowest mitochondrial membrane potential was observed in cells subjected to LDH/IOX1 and LDH treatments (Fig. 9), and this observation might be associated with aggregation of LDH particles.

To investigate whether the compounds are capable of modulating – besides cell viability – the proliferation potency of A549 as well, their anti-proliferative capacity was assessed using BrdU assay. Our results indicate that the proliferation of A549 cells was not affected by IOX1 and [RhCp*(LH)CI] treatments, as the number of BrdU-positive cells was similar to that obtained in the untreated control samples. Importantly, significantly lower BrdU incorporation was detected in the LDH/IOX1 and LDH-treated cells, suggesting a suppressed capability of cancer cell proliferation in these cases (Fig. 10).

As the tested compounds exhibited low cytotoxic activity against the non-small cell lung cancer cells (A549), which are known to be relatively redox- and drug-resistant, additional anti-proliferative assays were performed on human colorectal adenocarcinoma Colo205 cells that are more sensitive to metal chelators and redox-active compounds, using a longer incubation period. As expected, lower IC_{50} values were observed for the tested IOX1 and [RhCp*(LH)Cl] after 72 h of incubation (Table 5). Complexation with the RhCp* fragment significantly enhanced the cytotoxicity of IOX1, yielding an IC_{50} value of 15.13 μM.

In all, these results indicate that although all tested compounds decrease cancer cell viability and induce some damage to mitochondria, nevertheless, the rather strong toxicity of LDH/IOX1 and LDH, and the intensive mitochondrial damaging capacity, together with the necrosis triggering activity, LDH-containing agents, in their current form, are less suitable for drug loading purposes and that further formulation optimization, such as polyelectrolyte-based stabilization, will be necessary to mitigate aggregation-related effects.

Cytotoxicity of IOX1, [RhCp*(LH)Cl], TTM and deferiprone and their combinations on A549 tumor cells

Given the metal chelating ability of IOX1, we also aimed to explore the potential synergism with clinically relevant copper

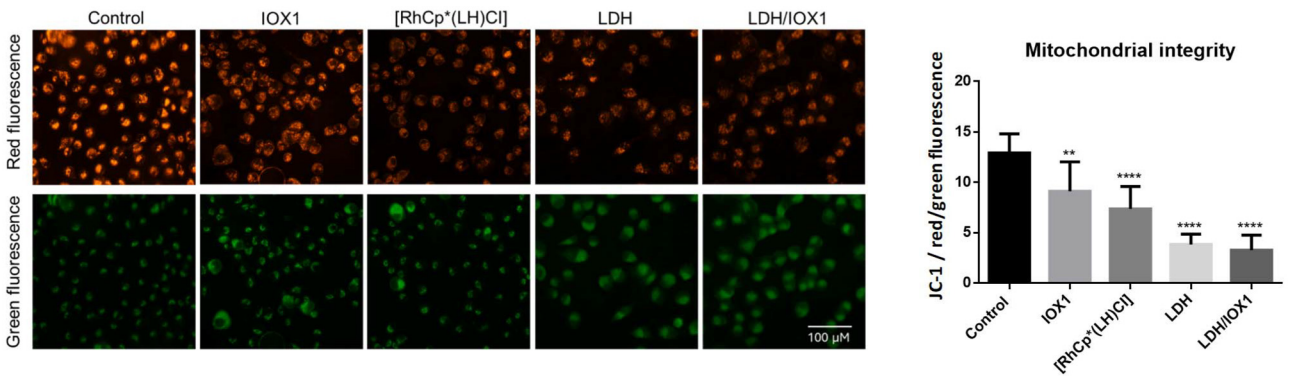

Fig. 9 The functional integrity of mitochondria in A549 cells upon IOX1, [RhCp*(LH)Cl], LDH, and LDH/IOX1 treatments was detected by JC-1 staining. One-way ANOVA, Dunnett's multiple comparisons test, $^{**}P < 0.005$, $^{****}P < 0.0001$.

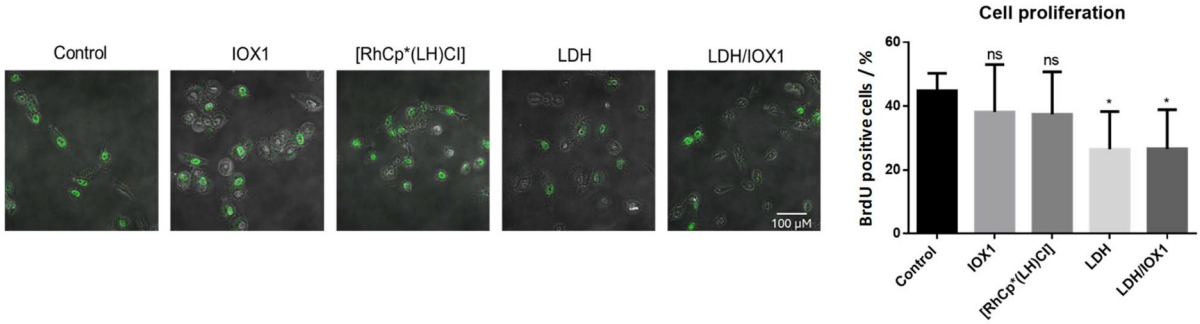

Fig. 10 Cell proliferation was determined upon IOX1, [RhCp*(LH)Cl], LDH, and LDH/IOX1 treatments on A549 cells. One-way ANOVA, Dunnett's multiple comparisons test, $*P < 0.05$.

and iron chelators such as TTM and deferiprone. The [RhCp*(LH)Cl] complex was also tested for comparison. For this, the toxicity of the individual compounds was assessed on A549 cells. To calculate the exact IC_{50} values, the same concentration range was applied (0, 100, 200, and 400 μM) for each compound. TTM and deferiprone were tested, and IOX1, as well as [RhCp*(LH)Cl], were examined again in parallel experiments. IOX1 significantly decreased the viability of A549 cells in all the tested concentrations, yielding the lowest IC_{50} value of all agents in this screen (Fig. S21). The RhCp* complex of IOX1 showed lower toxicity on A549 cells than IOX1, since [RhCp*(LH)Cl] affected the viability of tumor cells significantly only at higher concentrations. Similarly, TTM and deferiprone both had higher IC_{50} values than IOX1 (Table 5).

To detect whether the chelators have an impact on the toxic effect of IOX1 or [RhCp*(LH)Cl], combinational treatments were performed using the previously tested 100, 200, and 400 μM concentrations of each compound. The calculated combinational index (CI) values are shown in Tables S4–S7. The interaction between two drugs is additive when CI = 1, synergistic when CI < 1, and antagonistic when CI > 1.

At every tested concentration, the IOX1 and TTM show antagonistic interaction on A549 cells (Table S4). Similar to IOX1 and TTM combinations, antagonistic interaction was observed upon [RhCp*(LH)Cl] and TTM treatments as well (Table S5).

On the other hand, according to our results, deferiprone interacts synergistically with both IOX1 and [RhCp*(LH)Cl] at lower concentrations (Tables S6 and S7). Synergistic interaction was detected when one of the compounds was added at 100 μM concentration, and the other was applied in either 100 or 200 μM concentration (Tables S6 and S7). Additivity was observed between 400 μM [RhCp*(LH)Cl] and 100 μM deferiprone (Table S7). Interestingly, when IOX1 or [RhCp*(LH)Cl] was applied at higher concentrations, and either of them was combined with deferiprone, antagonism was detected between the two compounds (Tables S6 and S7).

In another analysis approach to reveal the interactions of IOX1 or [RhCp*(LH)Cl] with deferiprone or TTM, the effects of the drug combinations were investigated using constant concentration ratios of the compounds. In this case, the software reports the CI values based on certain effective dose values (ED), where ED_{50}, ED_{75}, ED_{90}, and ED_{95} are the doses required to achieve the desired effect in 50, 75, 90, or 95% of the cell population, respectively. IOX1 or [RhCp*(LH)Cl] in combination with TTM results in an antagonistic interaction at each ED value, such as at ED_{50}, ED_{75}, ED_{90}, and ED_{95} values (Table 6). Synergistic interaction was calculated between IOX1 or [RhCp*(LH)Cl] and deferiprone at ED_{50}. In all the other cases, antagonism was observed between the two compounds (Table 6).

Table 6 CI values calculated at ED_{50}, ED_{75}, ED_{90}, and ED_{95}

	CI values at ED_{50}	CI values at ED_{75}	CI values at ED_{90}	CI values at ED_{95}
IOX1 + TTM	1.26	1.90	3.57	5.92
[RhCp*(LH)Cl] + TTM	1.31	1.32	1.37	1.44
IOX1 + deferiprone	0.86	1.70	4.18	8.30
[RhCp*(LH)Cl] + deferiprone	0.97	1.84	3.64	5.90

These results confirm that even at constant ratios as well as non-constant concentration combinations of these agents, at lower concentrations, synergism can be verified between IOX1 or [RhCp*(LH)Cl] and deferiprone.

Conclusions

IOX1 is a metalloenzyme inhibitor with known biological activity; however, its interactions with essential metal ions have not been explored until now. Solution chemical properties of IOX1 were characterized by UV-vis and ^{1}H NMR techniques, as well as log D values characterizing lipophilicity were determined at different pH values. Based on the determined pK_a values, both the quinolinium nitrogen and the carboxyl group become deprotonated at physiological pH 7.4 in aqueous solution, resulting in the presence of the anionic LH^- form. This negatively charged form of IOX1 is hydrophilic, as evidenced by its negative log D value.

The interaction of IOX1 with Cu(II), Fe(III), and Fe(II) was investigated, and based on the determined overall stability constants, Cu(II) forms mono- and bis-complexes, while Fe(II) and Fe(III) also form tris-complexes with this ligand. A protonated mono-ligand complex was observed with Cu(II), whereas Fe(III) also forms a protonated bis-ligand species under acidic conditions. In these protonated complexes, the proton is attributed to the non-coordinating carboxyl group. Based on the calculated pM values, IOX1 shows the strongest preference for Cu(II) and a higher affinity for Fe(III) over Fe(II). This trend is consistent with that observed for other 8-hydroxyquinolines, such as HQ and HQS: Fe(II) < Fe(III) < Cu(II). The properties of redox-active complexes of IOX1 were investigated by cyclic voltammetry and UV-vis spectroelectrochemical measurements. Based on the obtained fairly negative formal potential values, IOX1 shows a preference for the higher oxidation states of the studied metal ions, such as Fe(III) and Cu(II), over the lower oxidation states. Both experiments confirmed that IOX1 has a higher affinity towards Fe(III) than Fe(II). The fact that IOX1 can form stable complexes with Fe(II) at physiological pH of 7.4 may still be sufficient for enzyme inhibition. A comparison of the determined overall stability constants for the natural substrate 2-oxoglutarate complexes with Fe(III) and Fe(II) clearly shows that IOX1 exhibits a higher affinity for both iron ions.

The half-sandwich [RhCp*(LH)Cl] complex of IOX1 was synthesized and characterized using NMR and ESI-MS techniques. The solution speciation studies revealed that the complex is stable over a wide pH range (pH 1.5–11.5) in aqueous solution, dissociation of IOX1 was not observed. At pH 7.4, [RhCp*(L)(H_2O)] form predominates, in which the carboxyl group is deprotonated.

The albumin binding of IOX1 and its RhCp* complex was investigated by spectrofluorometry, and for IOX1, complemented with ultrafiltration and equilibrium dialysis. Compared with other 5-substituted 8-hydroxyquinolines (HQCl and $HQNO_2$), IOX1 shows a lower affinity for HSA. In contrast, its RhCp* complex exhibits stronger albumin binding, as indicated by higher quenching constants. This enhanced interaction is consistent with the ability of the RhCp* complex to coordinate directly to albumin.

IOX1-loaded LDH nanoparticles were synthesized, and XRD measurements revealed that IOX1 did not intercalate between the layers but was instead bound to the LDH surface.

Anticancer properties of IOX1, RhCp* complex of IOX1, and LDH/IOX1 were evaluated on A549 and Colo205 human cancer cell lines. None of the compounds showed considerable cytotoxic activity after 24 h incubation on the A549 cells. The slightly increased cytotoxicity of the LDH-loaded IOX1 compared to the free IOX1 is attributed to the carrier itself, highlighting the need for further formulation optimization. Antiproliferative assays were performed with longer incubation times (72 h) on Colo205 cells. As expected, extending the incubation time resulted in lower IC_{50} values; moreover, a greater difference was observed between the IC_{50} values of IOX1 and its RhCp*complex. The latter exhibited higher activity (IC_{50} = 15.13 μM). Due to the strong metal chelation ability of 8-hydroxquinoline derivatives, the potential synergism of IOX1 with clinically relevant copper and iron chelators such as TTM and deferiprone was investigated. Synergism was verified between both IOX1 – deferiprone and [RhCp*(LH)Cl] – deferiprone combination at lower concentrations. An antagonistic effect was observed in all cases examined when the compounds were combined with TTM.

Materials and methods

Chemicals, stock solutions, and sample preparation

NaH_2PO_4, Na_2HPO_4, KH_2PO_4, NaCl, KCl, HNO_3, HCl, KOH, KNO_3, disodium-EDTA, $CuCl_2$, $FeCl_3$, *n*-octanol, and potassium hydrogen phthalate were obtained from Reanal or Molar Chemicals and used without further purification. Magnesium chloride hexahydrate ($MgCl_2{\cdot}6H_2O$), aluminium chloride hexahydrate ($AlCl_3{\cdot}6H_2O$), and sodium hydroxide pellet (NaOH) were purchased from VWR International. IOX1, Q-COOH, 2-OG, $[Rh(III)(\eta^6\text{-}C_5Me_5)(\mu\text{-}Cl)Cl]_2$, HSA (A8763, essentially globulin free and A1887 fatty acid free), DMF, DMSO, HEPES, maltol, warfarin, dansylglycine and 4,4-dimethyl-4-silapentane-1-sulfonic acid (DSS) were purchased from Sigma-Aldrich *in puriss* quality. All solvents were of analytical grade and used without further purification. Ultrapure water was used for sample preparation, which was produced by an ADRONA B30 or Milli-Q water purification system. The aqueous stock solutions of $[RhCp^*(H_2O)_3](NO_3)_2$ were obtained by dissolving an exact amount of the dimeric precursor in water, followed by the addition of equivalent amounts of $AgNO_3$, and the AgCl precipitate was filtered off. pH-Potentiometric measurements were performed to obtain the exact concentration of the precursor and ligand stock solutions. Cu(II) and Fe(III) stock solutions were prepared by dissolving the appropriate amount of the metal chlorides in known amounts of HCl. Their concentrations were determined by complexometry *via* the EDTA complexes. The Fe(II) stock solution was obtained from fine iron powder dissolved in a known amount of HCl solution under a purified, strictly oxygen-free argon atmosphere, then filtered, stored, and used under anaerobic conditions in a laboratory glove box (GP(Campus) Jacomex, O_2 content ≤ 1 ppm). KSCN solution was used to check the absence of Fe(III) traces in the Fe(II) solution. The concentration of the Fe(II) stock solution was determined by permanganometric titrations under acidic conditions. Accurate strong acid content of the metal stock solutions was determined by pH-potentiometric titrations. Modified phosphate-buffered saline (PBS′) solution was used to prepare HSA stock solutions. PBS′ contains 12 mM Na_2HPO_4, 3 mM KH_2PO_4, 1.5 mM KCl, and 100.5 mM NaCl; the concentrations of K^+, Na^+, and Cl^- ions correspond to the human blood serum. HSA concentration was calculated on the basis of their UV-vis absorption: λ_{280nm} (HSA) = 36 850 M^{-1} cm^{-1}.[57] Stock solutions of IOX1 were prepared in buffer (1 mM) for HSA binding studies. During the IOX1 and Q-COOH albumin binding studies PBS′ buffer was used, which also contained 2 mM EDTA.

Synthesis and characterization of the [RhCp*(IOX1)Cl] complex

IOX1 (7.83 mg, 32.35 μmol) was dissolved in a 1 : 1 methanol/chloroform mixture (30 mL), then half an equivalent of $[Rh(\eta^5\text{-}C_5Me_5)Cl_2]_2$ (10.00 mg, 16.18 μmol) and one equivalent of sodium methoxide were added. The reaction mixture was stirred for 12 h at room temperature, after which the solvent was partially evaporated and the product was precipitated by addition of dichloromethane. The resulting solid was collected by filtration and dried at 45 °C for 24 h. Yield: 8.62 mg (48.3%).

^{1}H NMR (DMSO-d_6, δ/ppm, Fig. S4): 12.177 (broad peak, 1H, Hlig(COOH)), 9.519 (d, J = 8.80 Hz, 1H, Hlig(4)), 8.835 (d, J = 4.74 Hz, 1H, Hlig(2)), 8.108 (d, J = 8.65 Hz; 1H Hlig(6)), 7.704 (m, 1H, Hlig(3)), 6.690 (d, J = 8.64 Hz, 1H, Hlig(7)), 1.655 (s, 15H, $HC_5Me_5(CH_3)$).

^{13}C NMR (DMSO-d_6, δ/ppm, Fig. S5): 173.33 (C(9)), 168.02 (C(8)), 148.30 (C(2)), 145.32 (C(8a)), 136.68 (C(6)), 136.46 (C(4)), 130.97 (C(4a)), 124.95 (C(3)), 113.12 (C(7)), 107.41 (C(5)), 93.83 ($C(C_5)$), 8.92; ($C(Me_5)$).

ESI-MS (water, positive, Fig. S3): calc. for $[RhCp^*(LH)]^+$ ($C_{20}H_{21}NO_3Rh$): 426.0576 (m/z) found: 426.0550 (m/z).

pH-Potentiometric measurements

pH-Potentiometric measurements were carried out to determine proton dissociation constants of the IOX1 and overall stability constants of 2-oxoglutarate complexes with Fe(II). For the complex formation of 2-oxoglutarate the measurements were performed in water with carbonate-free 0.10 M KOH, using 0.1 M KCl background electrolyte at 25.0 ± 0.1 °C as described in our previous works.[18,38] IOX1 ligand titration was performed in 30% (v/v) DMSO/H_2O solvent mixture. An Orion 710A pH-meter equipped with a Metrohm combined electrode (type 6.0234.100) and a Metrohm 665 Dosimat burette were used for the titrations. The electrode system was calibrated to the pH = $-\log[H^+]$ scale by means of blank titrations (HCl *vs.* KOH) according to the method suggested by Irving *et al.*[58] The average water ionization constant (pK_w) was 13.75 ± 0.01 in water and 14.53 in 30% (v/v) DMSO/H_2O, which is consistent with data found in the literature.[59] The pH-potentiometric titrations were performed in the pH range 2.0–11.7. Samples were deoxygenated by bubbling purified argon through them for *ca.* 10 min prior to the measurements. The sample's initial volume was 10.0 mL, and the ligand concentration was 2.0 mM. The accepted fitting of the titration curves was always less than 0.01 mL. pH-Potentiometric titrations were used to determine the exact concentration of the ligand stock solutions together with the proton dissociation constants using the computer program HYPERQUAD.[45] Quantitative ^{1}H NMR spectroscopy was performed for IOX1 using maltol as internal standard to determine its purity (≥96% (m/m)). The concentration of the prepared IOX1 stock solution was also calculated from its mass and volume, and showed good agreement with the values obtained from the pH-potentiometric titrations. HYPERQUAD[45] also used to determine the stoichiometry of the complexes and to calculate the formation constants ($\beta(M_pL_qH_r)$) in the case of 2-oxoglutarate. $\beta(M_pL_qH_r)$ is defined for the general equilibrium pM + qL + rH ⇌ $M_pL_qH_r$ as $\beta(M_pL_qH_r) = [M_pL_qH_r]/[M]^p[L]^q[H]^r$, where M denotes the metal ion and L the completely deprotonated ligand.

UV-visible spectrophotometric and fluorimetric measurements

A Thermo Evolution 220 spectrophotometer was used to record the UV-vis spectra at an interval of 190–1100 nm with a 1 cm path length. Spectrophotometric titrations were performed in water on samples containing IOX1 at 150–160 μM concentration, in the pH range from 1.5 to 11.7, in the absence or in the presence of 1, 0.5, or 0.33 equiv. metal ions (Cu(II), Fe(III) or Fe(II)). 2-OG–Fe(III) system was measured in the presence of 1,0.5, or 0.33 equiv. For Fe(III) ions, the data were evaluated at pH < 3 due to the sample precipitation. In the case of organometallic complex titration, it was performed with 1 to 1 ratio of RhCp* and IOX1. The ionic strength was adjusted with 0.2 M KNO_3 for the organometallic complex and 0.1 M KCl for the Fe(II/III) and Cu(II) complexes during the titrations. Spectrophotometric titrations with Fe(II) were done under strictly anaerobic conditions in a laboratory glove box. In this case, we used an Avantes spectrophotometer with an AvaLight-DHc light source and a 1 cm transmission dip probe. The proton dissociation (K_a), the overall stability constants ($\beta(M_pL_qH_r)$) and the individual spectra of the species were calculated with the computer program HypSpec[45] and for Fe(III) hydroxido species literature data were used ($\log\beta$ for $[MH_{-1}]$ = −2.20, $[MH_{-2}]$ = −5.71, $[MH_{-3}]$ = −12.26, $[MH_{-4}]$ = −21.60, $[M_2H_{-2}]$ = −2.91),[60] and for the Fe(II) hydroxide complexes ($\log\beta$ values, $[MH_{-1}]$ = −9.43, $[MH_{-2}]$ = −20.73, $[MH_{-3}]$ = −32.68 (ref. 60)). Hydrolysis constants were collected in Table S8. Concentration curves for the Fe(III)–IOX1 (1 : 3) system were calculated by using hydrolysis constants in various media, the curves are shown in Fig. S22.

The traditional shake-flask method was used to determine the values of the distribution coefficients ($\log D$) in *n*-octanol/water. Different types of buffers were used for the aqueous phase: 20 mM phosphoric acid, NaH_2PO_4 buffer at pH 2.0, and PBS′ buffer at pH 7.4 at 25.0 ± 0.2 °C as described previously.[61] 2 mM EDTA was added to the buffer solutions to avoid metal ion contamination.

Fluorescence studies were implemented by a Fluoromax (Horiba Jobin Yvon) fluorometer in 1 × 1 cm quartz cells. Samples contained 1 μM HSA or 1–1 μM HSA and site marker (WF, DG) in Trp214 quenching and site marker displacement experiments, respectively. Instrument settings are listed in Table S9. The computer program HypSpec[45] was utilized for the calculation of binding constants (K') for HSA–compound adducts, similar to the approach described in our former works.[61–63] Calculations were always based on data obtained from at least two independent measurements. Measured intensities were corrected for self-absorption and inner filter effect according to our former works using the formula suggested by Lakowicz.[46,62,64]

Electrospray ionization mass spectroscopy

Mass spectrometry measurements were carried out on a Micromass Q-TOF Premier (Waters MS Technologies) mass spectrometer equipped with electrospray ion source. Sample was prepared in NH_4HCO_3 buffer (pH = 7.4, c = 10 mM) and [RhCp*(LH)Cl] complex concentration was 200 μM.

NMR spectroscopy

^1H and ^{13}C NMR spectra were recorded on a Bruker AVANCE III HD Ascend 500 Plus instrument. For the complex characterization, the sample was prepared in 10 mM concentration in DMSO-d_6. ^{13}C NMR spectra was recorded with the attached proton test distinguishing CH and CH_3 as positive peaks and quaternary carbons and CH_2 as negative peaks. ^1H NMR spectroscopic titrations were performed in 10% (v/v) D_2O/H_2O mixture in the pH range 2.0–11.6 with KOH solution, and the ionic strength was 0.2 M (KNO_3). For ligand titration, IOX1 was dissolved at a concentration of 700 μM, while for titration of the $[RhCp^*(H_2O)_3]^{2+}$–IOX1 (1 : 1) system, the concentration was 500 μM. During the titrations, NMR spectra were recorded with the WATERGATE water supression pulse scheme.

Ultrafiltration and equilibrium dialysis

Samples were separated by ultrafiltration through 10 kDa membrane filters (Millipore, Amicon Ultra-0.5) into low and high molecular mass (LMM and HMM) fractions as described in our former work.[46] Samples contained 100 μM IOX1 and various equivalent HSA (0–165 μM). The concentration of the non-bound compounds in the LMM fractions was determined by UV-vis spectrophotometry (Agilent Cary 8454 diode array spectrophotometer) by comparing the recorded spectra to those of reference samples without the protein. The compound's adhesion to the filter (6%) was taken into account in our calculations.

The equilibrium dialysis experiments were conducted in PBS′ + 2 mM EDTA buffer at 25 °C using the same modified Rapid Equilibrium Dialysis (RED) inserts of Thermo Scientific™ as shown in our former work.[32] In this set the receiver compartment of the RED insert was removed, this way the dialysis bag (donor phase) containing the sample could be placed into a regular 1 cm quartz cuvette (acceptor phase) containing 2.00 mL buffer. The acceptor phase was continuously stirred and the release of the compounds into the buffer was monitored on-line in every 20 min without disrupting the layout using an Agilent Cary 3500 spectrophotometer equipped with eight-channel Peltier thermostable sample holder. The dialysis bag contained 0.30 mL sample: (i) site marker (100 μM WF or DG) or IOX1 (200 μM) only; (ii) HSA–site marker (1 : 1) or HSA–IOX1 (1 : 2); (iii) HSA–site marker–IOX1 (1 : 1 : 2) c_{HSA} was 100 μM. The whole device was capped with aluminium foil. All samples were done in duplicates. Detailed calculations are found in the SI.

Cyclic voltammetry and spectroelectrochemistry

Cyclic voltammograms were recorded for the Cu(II/I)–IOX1 and Fe(III/II)–IOX1 systems in 60% (v/v) DMF/H_2O solvent at 25.0 ± 0.1 °C using 0.1 M KNO_3 as supporting electrolyte. The pH of the samples was adjusted to 7.4 using HCl/KOH solutions. The concentration of the metal ion was 0.5 mM, and 1 : 3 or 1 : 2 metal-to-ligand ratios were used. Measurements were performed on a three-electrode system: glassy carbon, platinum, and Leakless Ag|AgCl were used as working, auxiliary, and reference electrodes. Autolab PGSTAT 204 potentiostat/galvanostat was used with Metrohm's Nova software (version 2.0, Metrohm Autolab B.V.). Samples were purged with argon for *ca.* 10 minutes before recording the voltammograms.

Spectroelectrochemical measurements were performed by using a spectroelectrochemical cell kit (AKSTCKIT3) with the Pt-microstructured honeycomb electrode (as working and auxiliary electrode) and LowProfile Ag/AgCl electrode as reference electrode (Pine Research Instrumentation). The special quartz cell with 1.70 mm optical path length was positioned in the CUV-UV cuvette holder connected to the diode-array UV-vis spectrometer (Avantes, Model AvaLight-DHc light source equipped with an AvaSpec-UL2048XL-EVO) by optical fibers. AvaSoft 8.1.1 software package (Avantes) was used to collect the spectra.

Synthesis, structural and morphological characterization of the IOX1-loaded LDH nanoparticles

LDH nanoparticles were synthesized by the coprecipitation method.[65] In brief, 5 mL of 0.8 M (3 : 1 Mg(II)-to-Al(III) ratio) metal salt solution was mixed with 20 mL NaOH solution (0.4 M) under N_2 atmosphere with vigorous stirring. The reaction mixture was stirred for 40 min, then centrifuged and washed three times with ultrapure water. Finally, the slurry was redispersed and used for further measurements.

IOX1-loaded nanoparticles (denoted as LDH/IOX1) were synthesized following the same protocol, except that IOX1 was dissolved in the initial NaOH solution in 1 mM concentration. The obtained dispersion was treated in the same way as the bare LDH dispersion.

A Phillips PW 1830 diffractometer with Cu Kα radiation source (λ = 0.1542 nm) was used to record the X-ray diffractograms and characterize the crystal structure of the nanoparticles. The diffractograms were recorded in 5–80 2θ range with 0.02° interval. The primer crystallite size (τ) was determined by the Scherrer equation:[66]

$$\tau = \frac{K \times \lambda}{\beta \times \cos\theta} \quad (1)$$

where K is the shape factor, β is the full width at half maximum, while θ is the angle of the reflection.

SHIMADZU UC-3600i Plus UV-VIS-NIR spectrophotometer was used to record to UV-vis spectra of the solid samples. The device is equipped with PMT, InGaAs, and PbS detectors. The data were recorded in the 200–800 nm range with 0.1 nm resolution.

A Jeol JEM-1400Plus transmission electron microscope (TEM) was used to determine the morphology of the samples. 10 μL of the dispersion of each sample was dropped onto a carbon-coated Formvar foil 200 mesh copper grid and dried at room temperature. To determine the size distribution and average diameter of the nanoparticles, the size of 150 individual particles was measured using ImageJ software.

Determination of size and charge of the IOX1-loaded LDH nanoparticles

Litesizer 500 instrument (Anton Paar) was used to perform dynamic light scattering (DLS) and electrophoretic light scattering (ELS) measurements to determine the size and the charge of the nanoparticles in aqueous dispersions. The instrument operates with a λ = 685 nm laser and 40 mW power. The experiments were performed at 25 °C and 175° scattering angle in disposable plastic cuvettes (VWR International). The hydrodynamic radius (R_h) values were calculated from the translational diffusion coefficient (D) data with the Stokes–Einstein equation:[67]

$$R_h = \frac{k_B \times T}{6 \times \pi \times \eta \times D} \quad (2)$$

where T is the absolute temperature, and η is the dynamic viscosity of the solvent.

ELS measurements were carried out in Ω-shaped plastic cuvettes using 1 mM NaCl as background electrolyte. The zeta potential (ζ) values were calculated from the electrophoretic mobilities (μ) with the Smoluchowski equation:[68]

$$\mu = \frac{\varepsilon \times \varepsilon_0 \times \zeta}{\eta} \quad (3)$$

where ε is the relative permittivity of water and ε_0 is the permittivity of the vacuum.

Determination of the IOX1 concentration in the IOX1-loaded LDH nanoparticles

The concentration of IOX1 anchored on the LDH nanoparticles was determined by UV-vis using a GENESYS 10S spectrophotometer. Here, 1 mL of LDH/IOX1 dispersion was dissolved in 1 M HCl solution, and then, the absorbance data were collected in the wavelength range of 250–500 nm (Fig. S24a). The calibration curve of IOX1 was recorded within 0–0.6 mM concentration regime. In these samples, an HCl concentration of 0.32 M was kept constant by the addition of calculated amount of 1 M HCl solution. The IOX1 concentration was calculated using the calibration curve determined (Fig. S24b).

Cell culture and cell viability assay

A549 human lung adenocarcinoma and Colo205 human colorectal adenocarcinoma cell lines were purchased from ATCC. A549 cells were maintained in Dulbecco's Modified Eagle's medium (DMEM, Biosera, Cholet, France) containing 1 g L^{-1} glucose, and Colo205 cells were cultured in RPMI 1640 medium (Biosera, Cholet, France) complemented with 10% fetal bovine serum (FBS, EuroClone, Pero, Italy), 2 mM glutamine (Sigma-Aldrich, St Louis, Missouri, USA), 0.01% streptomycin, and 0.006% penicillin (Biosera, Cholet, France). Cells were cultured under standard conditions in a 37 °C incubator containing 5% CO_2 and 95% humidity.

To detect the cell viability of A549 cells upon IOX1, [RhCp*(LH)Cl], LDH, and LDH/IOX1, MTT assay was performed. Stock solutions of IOX1 and [RhCp*(LH)Cl] were prepared in 50% (v/v) DMSO/H_2O at a concentration of 6 mM. The LDH/IOX1 stock dispersion contained 0.6 mM IOX1 and 10.7 g L^{-1} LDH, while the LDH stock dispersion was prepared at 11.0 g L^{-1}. For this, cells were seeded into 96-well plates at a 1×10^4 cell per well density. On the following day, the cells were treated with increasing concentrations of compounds (0, 50, 100, 200, 300 μM) for 24 h.

For the detection of synergistic, additive, or antagonistic interaction between IOX1, [RhCp*(LH)Cl], in combination with iron chelator: deferiprone or copper chelator TTM, cells were treated with either IOX1, [RhCp*(LH)Cl], TTM, deferiprone, or the combination of these drugs for 24 h. Since different concentrations of each agent may have different interactions with the others, each treatment concentration of the agents was tested separately. Each substance was used at concentrations of 0, 100, 200, and 400 μM, and the agents in different concentrations were combined.

The antiproliferative and cytotoxic effects of IOX1 and [RhCp*(LH)Cl] on Colo205 cells were also investigated using the MTT assay. For this, 5000 cells were seeded into each well of a 96-well plate and left to grow. On the following day, the cells were treated with increasing concentrations of IOX1 and [RhCp*(LH)Cl] (0, 25, 50, 100, and 200 μM) for 72 h.

After the treatments, cells were washed with phosphate-buffered saline (PBS, pH 7.4) and then incubated with 0.5 mg mL^{-1} MTT (Sigma-Aldrich, St Louis, Missouri, USA) containing culture medium for 1 h at 37 °C. Formazan crystals were solubilized in dimethyl sulfoxide (DMSO, Serva Electrophoresis GmbH, Heidelberg, Germany), and the absorbance was determined using a Synergy HTX plate reader (BioTek, Winooski, Vermont, USA) at 570 nm. MTT measurements were repeated three times using at least four independent replicates. The viability of the untreated control samples was considered 100% upon data analysis. IC_{50} values were estimated in GraphPad Prism 6 software, and combinational indices (CI) were calculated by CompuSyn (version 1.0, ComboSyn Inc.) to investigate the synergistic, additive, or antagonistic effect of combinational drug treatments.

Lactate dehydrogenase release assay

To detect the toxicity of compounds on tumor cells, the release of lactate dehydrogenase was measured from the supernatant of the samples by Cayman Lactate dehydrogenase Cytotoxicity Assay Kit (Cayman Chemicals, Ann Arbor, Michigan, USA). For this, 1×10^4 A549 cells per well were seeded into a 96-well plate and left to grow. On the following day, the cells were treated with 150 μM of IOX1, [RhCp*(LH)CI], LDH, or LDH/IOX1 for 24 h. After the incubation, 100 μL of supernatant was

transferred to a new 96-well plate and incubated for 30 min with Lactate dehydrogenase Reaction Solution prepared according to the instructions of the manufacturer. As a positive control, cell lysate samples were prepared using Triton-X-100 according to the instructions of the manufacturer. The absorbance of the samples was measured with Synergy HTX plate reader (BioTek, Winooski, Vermont, USA) at 490 nm. The lactate dehydrogenase release (%) of the samples was calculated, with the lactate dehydrogenase release of the positive control sample considered as 100%.

Cell proliferation assay

Cell proliferation following treatment of A549 cells with IOX1, [RhCp*(LH)Cl], LDH, or LDH/IOX1 was investigated using 5-bromo-2′-deoxy-uridine (BrdU) Labeling and Detection Kit I (Roche, Cat. No. 11 296 736 001, Basel, Switzerland). For this, 3×10^4 cells were seeded onto glass coverslips (VWR International, Radnor, Pennsylvania, USA) placed onto 24-well plates. On the following day, the samples were treated with 50 μM of each compound for 24 h. After the incubation, BrdU labeling solution was added at a 1 : 1000 dilution for 30 min. Then the samples were fixed with Ethanol Fixative solution (70% ethanol diluted in 50 mM glycine solution, pH 2.0) and the protocol for adherent cells was performed according to the manufacturer's instructions. BrdU incorporation was detected with an Olympus FV10i confocal microscope (Olympus, Tokyo, Japan).

Assessment of mitochondrial health

The mitochondria-damaging effect of the compounds was investigated by JC-1 staining. For the JC-1 staining, 1×10^5 cells per well were seeded onto glass coverslips (VWR International, Radnor, Pennsylvania, USA) in a 24-well plate. The next day, the cells were treated with 150 μM of either IOX1, [RhCp*(LH)Cl], LDH, or LDH/IOX1 for 24 h. After the treatments, the cells were washed in PBS, and JC-1 dye (Thermo Fisher Scientific, Waltham, Massachusetts, USA) dissolved in DMSO (Serva Electrophoresis, Heidelberg, Germany) was added in 10 μg mL^{-1} final concentration diluted in full culture media. After 15 min incubation, the cells were washed three times with PBS and visualized by an OLYMPUS BX51 microscope with an Olympus DP70 camera (Olympus, Tokyo, Japan). The red and green fluorescence intensity was quantified using ImageJ software.

Conflicts of interest

There are no conflicts to declare.

Data availability

The data supporting this article have been included as part of the supplementary information (SI). Supplementary information: ^{1}H and ^{13}C NMR, ESI-MS, UV-vis and fluorescence spectra, cyclic voltammograms, characterization data for the LDH-based nanoparticles (TEM, DRS, zeta potential, *etc.*), viability data, CI values and tables for the equilibrium dialysis and steady-state fluorometric measurements. See DOI: https://doi.org/10.1039/d6dt00242k.

Acknowledgements

The work was supported by the National Research, Development and Innovation Fund through projects NANO-IBD 2024-1.2.3-HU-RIZONT-2024-00035, OTKA-NKFIH (K142371, M. K.), and the Incubation Competence Centre of the Centre of Excellence for Interdisciplinary Research, Development and Innovation of the University of Szeged (N. I., C. B.). N. I. was supported by the János Bolyai Research Fellowship of the Hungarian Academy of Sciences (BO/00351/22/8).

References

1 S. G. Nerella, P. S. Thacker, M. Arifuddin and C. T. Supuran, *Eur. J. Med. Chem. Rep.*, 2024, **10**, 100131.
2 J. Hu, P. E. Van den Steen, Q.-X. A. Sang and G. Opdenakker, *Nat. Rev. Drug Discovery*, 2007, **6**, 480.
3 Q. Wu, B. Young, Y. Wang, A. M. Davidoff, Z. Rankovic and J. Yang, *J. Med. Chem.*, 2022, **65**(14), 9564.
4 T. E. McAllister, K. S. England, R. J. Hopkinson, P. E. Brennan, A. Kawamura and C. J. Schofield, *J. Med. Chem.*, 2016, **59**(4), 1308.
5 A. R. Joaquim, M. P. Gionbelli, G. Gosmann, A. M. Fuentefria, M. S. Lopes and S. Fernandes de Andrade, *J. Med. Chem.*, 2021, **64**(22), 16349.
6 R. Gupta, V. Luxami and K. Paul, *Bioorg. Chem.*, 2021, **108**, 104633.
7 H. A. Saadeh, K. A. Sweidan and M. S. Mubarak, *Molecules*, 2020, **25**, 4321.
8 V. F. S. Pape, A. Gaál, I. Szatmári, N. Kucsma, N. Szoboszlai, C. Streli, F. Fülöp, É. A. Enyedy and G. Szakács, *Cancers*, 2021, **13**, 154.
9 Y. Song, H. Xu, W. Chen, P. Zhan and X. Liu, *MedChemComm*, 2015, **6**, 61.
10 ClinicalTrials.gov can be found under https://clinicaltrials.gov/study/NCT04143789, (accessed: 26/01/2026).
11 R.-D. Hofheinz, C. Dittrich, M. A. Jakupec, A. Drescher, U. Jaehde, M. Gneist, N. Graf, V. Keyserlingk, B. K. Keppler and A. Hochhaus, *Int. J. Clin. Pharmacol. Ther.*, 2005, **43**, 590.
12 Y. Yang, L.-Q. Du, Y. Huang, C.-J. Liang, Q.-P. Qin and H. Liang, *J. Inorg. Biochem.*, 2023, **241**, 112152.
13 M. N. Alam, M. A. Moni, J. Q. Yu, P. Beale, P. Turner, N. Proschogo, M. A. Rahman, M. P. Hossain and F. Huq, *Int. J. Mol. Sci.*, 2021, **22**, 8471.
14 T. Pivarcsik, S. Tóth, S. P. Pósa, N. V. May, É. Kováts, G. Spengler, I. Kántor, A. Rolya, T. Feczkó, I. Szatmári,

G. Szakács and É. A. Enyedy, *Inorg. Chem.*, 2024, **63**(50), 23983.
15 T. Pivarcsik, O. Dömötör, J. P. Mészáros, N. V. May, G. Spengler, O. Csuvik, I. Szatmári and É. A. Enyedy, *Int. J. Mol. Sci.*, 2021, **22**, 11281.
16 T. R. Steel, J. Stjärnhage, Z. Lin, H. O. Bloomfield, C. D. Herbert, J. W. Astin, K. Krawczyk, B. Rychlik, D. Plażuk, S. M. F. Jamieson and C. G. Hartinger, *Dalton Trans.*, 2025, **54**, 1583.
17 W. D. J. Tremlett, K. K. H. Tong, T. R. Steel, S. Movassaghi, M. Hanif, S. M. F. Jamieson, T. Söhnel and C. G. Hartinger, *J. Inorg. Biochem.*, 2019, **199**, 110768.
18 O. Dömötör, V. F. S. Pape, N. V. May, G. Szakács and É. A. Enyedy, *Dalton Trans.*, 2017, **46**, 4382.
19 V. F. S. Pape, R. Palkó, S. Tóth, M. J. Szabó, J. Sessler, G. Dormán, É. A. Enyedy, T. Soós, I. Szatmári and G. Szakács, *J. Med. Chem.*, 2022, **65**(11), 7729.
20 V. Prachayasittikul, S. Prachayasittikul, S. Ruchirawat and V. Prachayasittikul, *Drug Des., Dev. Ther.*, 2013, **7**, 1157.
21 A. Cipurković, E. Horozić, S. Marić, L. Mekić and H. Junuzović, *Open J. Appl. Sci.*, 2021, **11**, 1.
22 G. Szakács, M. D. Hall, M. M. Gottesman, A. Boumendjel, R. Kachadourian, B. J. Day, H. Baubichon-Cortay and A. Di Pietro, *Chem. Rev.*, 2014, **114**(11), 5753.
23 H. Kovács, T. Jakusch, N. V. May, S. Tóth, G. Szakács and É. A. Enyedy, *J. Inorg. Biochem.*, 2024, **255**, 112540.
24 R. J. Hopkinson, A. Tumber, C. Yapp, R. Chowdhury, W. Aik, K. H. Che, X. S. Li, J. B. L. Kristensen, O. N. F. King, M. C. Chan, K. K. Yeoh, H. Choi, L. J. Walport, C. C. Thinnes, J. T. Bush, C. Lejeune, A. M. Rydzik, N. R. Rose, E. A. Bagg, M. A. McDonough, T. J. Krojer, W. W. Yue, S. S. Ng, L. Olsen, P. E. Brennan, U. Oppermann, S. Müller, R. J. Klose, P. J. Ratcliffe, C. J. Schofield and A. Kawamura, *Chem. Sci.*, 2013, **4**, 3110.
25 R. G. Hoyle, H. Wang, Y. Cen, Y. Zhang and J. Li, *Mol. Cancer Ther.*, 2021, **20**, 191.
26 S. Fang, H. Cao, J. Liu, G. Cao and T. Li, *Int. Immunopharmacol.*, 2024, **141**, 112896.
27 S. Amézqueta, J. L. Beltrán, A. M. Bolioli, L. Campos-Vicens, F. J. Luque and C. Ràfols, *Pharmaceuticals*, 2021, **14**, 214.
28 J. Fan, K. Gilmartin, S. Octaviano, F. Villar, B. Remache and J. Regan, *ACS Pharmacol. Transl. Sci.*, 2022, **5**(9), 803.
29 R. Sun, J. Xiang, Q. Zhou, Y. Piao, J. Tang, S. Shao, Z. Zhou, Y. H. Bae and Y. Shen, *Adv. Drug Delivery Rev.*, 2022, **191**, 114614.
30 V. K. Ameena Shirin, R. Sankar, A. P. Johnson, H. V. Gangadharappa and K. Pramod, *J. Controlled Release*, 2021, **330**, 398.
31 J. Wen, K. Yang, J. Huang and S. Sun, *Mater. Des.*, 2021, **198**, 109298.
32 E. F. Várkonyi, S. Tóth, T. Pivarcsik, O. Dömötör, O. Berkesi, N. V. May, G. Szakács, E. Csapó and É. A. Enyedy, *Inorg. Chem.*, 2025, **64**, 14914.
33 T. Feng, D. Li, H. Wang, J. Zhuang, F. Liu, Q. Bao, Y. Lei, W. Chen, X. Zhang, X. Xu, H. Sun, Q. You and X. Guo, *Eur. J. Med. Chem.*, 2015, **105**, 145.
34 SCQuery, *The IUPAC Stability Constants Database, Academic Software (version 5.5)*, Royal Society of Chemistry, 1993–2005.
35 M. Born, *Z. Phys.*, 1920, **1**, 45.
36 X. Yang, S. Bi, X. Wang, J. Liu and Z. Bai, *Anal. Sci.*, 2003, **19**, 273.
37 T. D. Turnquist and E. B. Sandell, *Anal. Chim. Acta*, 1968, **42**, 239.
38 T. H. Vu, N. Serradji, M. Seydou, É. Brémond and N. Ha-Duong, *J. Inorg. Biochem.*, 2020, **203**, 110864.
39 V. F. S. Pape, N. V. May, G. T. Gál, I. Szatmári, F. Szeri, F. Fülöp, G. Szakács and É. A. Enyedy, *Dalton Trans.*, 2018, **47**, 17032.
40 I. Dellien, *Acta Chem. Scand.*, 1977, **31a**, 473.
41 J. T. Smith and V. M. Doctor, *J. Inorg. Nucl. Chem.*, 1975, **37**, 775.
42 J. P. Mészáros, J. M. Poljarević, I. Szatmári, O. Csuvik, F. Fülöp, N. Szoboszlai, G. Spengler and É. A. Enyedy, *Dalton Trans.*, 2020, **49**, 7977.
43 J. P. Mészáros, G. Németi, J. M. Poljarevic, T. Holczbauer, N. V. May and É. A. Enyedy, *Eur. J. Inorg. Chem.*, 2021, 1858.
44 O. Dömötör, T. Pivarcsik, Z. N. Yazdi, É. Bakos, C. Özvegy-Laczka, A. Hetényi, T. Martinek, I. Szatmári, S. Tóth, G. Szakács, A. Borics and É. A. Enyedy, *Eur. J. Pharm. Sci.*, 2025, **212**, 107187.
45 P. Gans, A. Sabatini and A. Vacca, *Talanta*, 1996, **43**, 1739.
46 O. Dömötör and É. A. Enyedy, *J. Biol. Inorg. Chem.*, 2019, **24**, 703.
47 W. Hu, Q. Luo, X. Ma, K. Wu, J. Liu, Y. Chen, S. Xiong, J. Wang, P. J. Sadler and F. Wang, *Chem. – Eur. J.*, 2009, **15**, 6586.
48 T. Pivarcsik, V. Pósa, H. Kovács, N. V. May, G. Spengler, S. P. Pósa, S. Tóth, Z. N. Yazdi, C. Özvegy-Laczka, I. Ugrai, I. Szatmári, G. Szakács and É. A. Enyedy, *Int. J. Mol. Sci.*, 2023, **24**, 593.
49 J. Wen, K. Yang, X. Ding, H. Li, Y. Xu, F. Liu and S. Sun, *Inorg. Chem.*, 2019, **58**, 2987.
50 M. B. Engelhardt, T. Sugimoto, G. Papastavrou and M. Kobayashi, *Colloids Surf., A*, 2024, **703**, 135244.
51 A. M. Smith, M. Borkovec and G. Trefalt, *Adv. Colloid Interface Sci.*, 2020, **275**, 102078.
52 Z. Zachariah, M. P. Heuberger and R. M. Espinosa-Marzal, *One Hundred Years of Colloid Symposia: Looking Back and Looking Forward, ACS Symposium Series*, 2023, vol. 1457, pp. 31–47.
53 L. H. Hanus and H. J. Ploehn, *Langmuir*, 1999, **15**, 3091.
54 N. A. Jose, H. C. Zeng and A. A. Lapkin, *Nat. Commun.*, 2018, **9**, 4913.
55 A. Szerlauth, Z. D. Kónya, G. Papp, Z. Kónya, Á. Kukovecz, M. Szabados, G. Varga and I. Szilágyi, *J. Colloid Interface Sci.*, 2023, **632**, 260.
56 O. N. F. King, X. S. Li, M. Sakurai, A. Kawamura, N. R. Rose, S. S. Ng, A. M. Quinn, G. Rai, B. T. Mott, P. Beswick, R. J. Klose, U. Oppermann, A. Jadhav, T. D. Heightman, D. J. Maloney, C. J. Schofield and A. Simeonov, *PLoS One*, 2010, **5**, e15535.

57 G. H. Beaven, S.-H. Chen, A. D'albis and W. B. Gratzer, *Eur. J. Biochem.*, 1974, **41**, 539.
58 H. M. Irving, M. G. Miles and L. D. Pettit, *Anal. Chim. Acta*, 1967, **38**, 475.
59 L. D. Pettit and K. J. Powell, *IUPAC Stability Constant Database*, IUPAC/Academic Software, Otley, (UK), 1993.
60 P. L. Brown and C. Ekberg, *Hydrolysis of Metal Ions*, Wiley, 2016, pp. 135–145.
61 E. A. Enyedy, D. Hollender and T. Kiss, *J. Pharm. Biomed. Anal.*, 2011, **54**, 1073.
62 O. Dömötör, C. G. Hartinger, A. K. Bytzek, T. Kiss, B. K. Keppler and E. A. Enyedy, *J. Biol. Inorg. Chem.*, 2013, **18**, 9.
63 É. A. Enyedy, O. Dömötör, K. Bali, A. Hetényi, T. Tuccinardi and B. K. Keppler, *J. Biol. Inorg. Chem.*, 2015, **20**, 77.
64 J. R. Lakowicz, *Principles of Fluorescence Spectroscopy*, 3rd edn, Springer, New York, 2006.
65 C. Dazon, C. Taviot-Guého and V. Prévo, *Mater. Adv.*, 2023, **4**, 4637.
66 Y. Zhao, F. Li, R. Zhang, D. G. Evans and X. Duan, *Chem. Mater.*, 2002, **14**, 4286.
67 P. A. Hassan, S. Rana and G. Verma, *Langmuir*, 2015, **31**, 3.
68 A. V. Delgado, F. González-Caballero, R. J. Hunter, L. K. Koopal and J. Lyklema, *J. Colloid Interface Sci.*, 2007, **309**, 194.